ELECTRICAL DISCHARGE TEXTURING FOR VIBRATION CONTOL

ELECTRICAL DISCHARGE TEXTURING FOR VIBRATION CONTROL

BY

FELIPE PEREIRA COELHO, B.Eng.

A THESIS

SUBMITTED TO THE DEPARTMENT OF MECHANICAL ENGINEERING

AND THE SCHOOL OF GRADUATE STUDIES

OF MCMASTER UNIVERSITY

IN PARTIAL FULFILMENT OF THE REQUIREMENTS

FOR THE DEGREE OF

MASTER OF APPLIED SCIENCE

Master of Applied Science (2021) McMaster University

(Mechanical Engineering) Hamilton, Ontario, Canada

TITLE: Electrical Discharge Texturing for Vibration Control

AUTHOR: Felipe Pereira Coelho

B. Eng. (Mechanical Engineering)

Universidade Estadual Paulista – "Julio de Mesquita Filho" – UNESP.

SUPERVISOR: Dr. Philip Koshy

NUMBER OF PAGES: 105

To Rep. Acapulco, Bauru-SP

Where I made friends for life.

Abstract

Self-excited vibration, known as chatter, limits material removal rate, surface finish and accuracy in machining, and may even cause structural damage to components of the machining system. Machining stability may be enhanced by a variety of methods, from moving machining parameters to stable regions, or using actively actuated tools specially designed to obstruct self-excitation, or even by passively enhancing the stiffness or damping of the system as to soften the critical mode of vibration. Although there are many approaches to reduce chatter, not all of them are always effective in every situation. Moving machining parameters is restricted by workpiece machinability. Active damping mechanisms require large contraptions to function and have limited effectiveness when dealing with high frequency chatter. Passive damping approaches have essentially entailed tuned mass dampers which require delicate finetuning and drastic alterations to the tool structure in order mount the vibration absorber system. This research presents an elegant and innovative application involving electrical discharge texturing for chatter suppression that takes advantage of frictional forces to passively damp self-excited vibrations. This technique proved effective in a frequency range from 100 to 4000 Hz achieving damping enhancements of more than 400% without the need of any tuning and showing repeatable damping values after subsequent assembly and disassembly cycles. When applied to a grooving operation the technique proved effective in increasing the limiting width of cut by more than 120%.

Acknowledgments

This degree comes not without the help of many people. I would not be here if not for the help, guidance and knowledge given to me by numerous people. The list of which is far too long to fit in these pages. With that being said, I would like to at the very least acknowledge my gratitude and appreciation to as many of those people that I can, in the space that I have. I would like to start by expressing my sincere gratitude to my supervisor Dr. Philip Koshy, for all the help he has given me throughout this research. His patience and guidance helped me overcome numerous challenges. The knowledge he so kindly shared with me has made me grow as a person and an engineer. I'm extremely thankful for all that he has taught me throughout these years.

I would like to extend my sincere gratitude to Brady Sample, for all the knowledge he shared with me, all the advice he gave me, as well as for all the attention and all the time he invested in helping me overcome many, many, problems.

I would like to express my sincere gratitude to Nicole McLean, for her time, attention and patience, helping me from day one.

I would like to acknowledge and express my gratitude to Alam Shafiul, for helping me with the tap tests and the measurement equipment, as well as to Mohammad Shariful for patiently helping me scan numerous eroded surfaces.

I would like to acknowledge Tarcisio, Max, Lucas, Luca and Maxwell, for all the coffees, beers and talks we had through these years. I'm thankful for having met you guys.

I would like to express my sincere gratitude to my causing Eric, his wife Carol and their two daughters Ana Julia and Ana Cecilia, for all their support during some difficult times through these two years. Thank you for all the weekend getaways.

I would like to express from the bottom of my heart my most sincere gratitude and appreciation to my girlfriend Beatriz, for the more than 2000 video calls where she was always supportive and patient throughout all the challenges that we faced while 12 thousand kilometres apart for these 2 years.

Finally, I would like to thank my parents and my brother, for all their support, advice and love.

Contents

List of Figures

List of Tables

Chapter 1

1 Introduction

Machining processes often encounters vibration problems. The most common of these is chatter, which can lead to undesirable surface finish (Figure 1.1) as well as damage to the cutting tool and even the machine tool. Slender tools encounter excessive deflections under machining forces, which create a varying force on the tool that leads to regenerative vibrations. There are two avenues to solving such a problem: increasing the tool stiffness or enhancing its damping. Increasing stiffness can only be done by changing the geometry or the material of the tool, which may not be always possible. Machining processes such as boring require tools with a large length-to-diameter ratio as these are used to generate internal features in a workpiece. Similarly, parting tools are often required to be long and narrow. Changing the tool material can only go so far since tools are already made from materials with high Young's modulus; furthermore, increasing the Young's modulus is often accompanied by an increase in density that increases the vibrating mass. This leaves an increase in damping to be the remaining alternative.

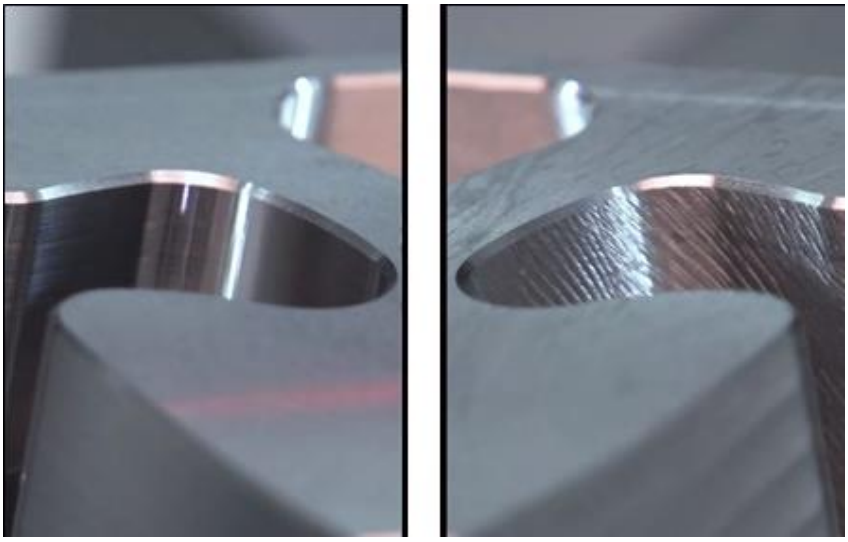

(a) (b)

Figure 1.1 Surface finish without chatter. b) Surface finish with chatter. [1]

Damping can be increased using approaches that are either passive or active. Passive techniques are different from their active counterparts in that they damp vibrations without the use of any external power. Passive techniques include various approaches to dissipate vibrational energy, some examples being impact dampers [2], friction dampers [3] and tuned mass dampers [4]. This thesis presents research that develops a passive technique involving friction damping that takes advantage of a phenomenon known as micro-slip.

Micro-slip is generally found in joint interfaces such as in bolted structures, in the region adjacent to the bolt called the slip region [5,6]. The hypothesis in the present research is that micro-slip may be enhanced by engineering the surfaces comprising a joint in terms of its skewness characteristics, by using Electrical Discharge Machining

(EDM). Among machining processes, EDM is unique in that it is capable of generating isotropic rough surfaces with a positively skewed surface height distribution.

The rest of this chapter reviews the mechanism of chatter encountered in orthogonal machining processes, provides a brief overview of the micro-slip phenomenon as a damping mechanism, and the essential details of material removal using EDM.

1.1Chatter

During orthogonal machining operations two forces act on the cutting tool: one in the radial direction (Fr) and another in the tangential direction (Ft). These forces are proportional to the uncut chip thickness (h) and the cutting width (w) and so variations in uncut chip thickness (Δh) lead to variations in the cutting forces on the tangential direction (ΔF_t) and in the feed direction (ΔF_f), as expressed by equations 1.1 and 1.2.

$$\Delta F_t = K_{ct} \cdot w \cdot \Delta \mathrm{h} \tag{1.1}$$

$$\Delta F_f = K_{cf} \cdot w \cdot \Delta \mathrm{h} \tag{1.2}$$

When a tool first engages the workpiece, it deflects due to the forces encountered. This drives the tool into a state of vibration, moving it towards and away from the workpiece, often without disengaging from the work. This motion over the workpiece surface imprints a wave pattern which the tool will encounter during subsequent revolutions. Chatter results when the frequency of this wave pattern does not match the

tool vibrational frequency. The frequency and amplitude of these wave patterns are a function of the workpiece rotational speed, and the tool stiffness and damping characteristics. Figure 1.2 illustrates how tool deflection imprints wave patterns on the workpiece surface.

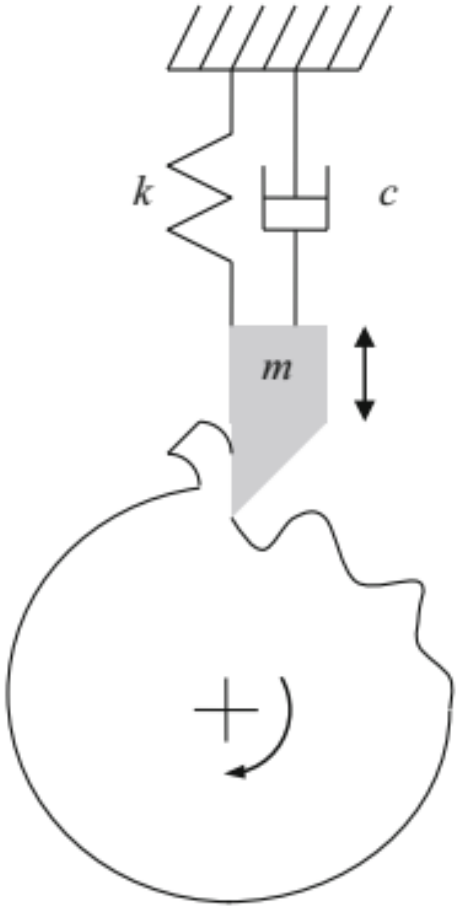

Figure 1.2 Wave imprints caused by tool deflection [7].

As already alluded to, this research investigated passive damping to mitigate tool chatter by exploiting the phenomenon of micro-slip, which is discussed next.

1.2Micro-slip

Bolted structures exhibit higher damping than their monolithic equivalents. The increase in damping originates at the joint interface. The joint interface under the influence of clamping force [4,5] can be divided into two regions: a sticking region and a slipping region [4,5] (Figure 1.3).

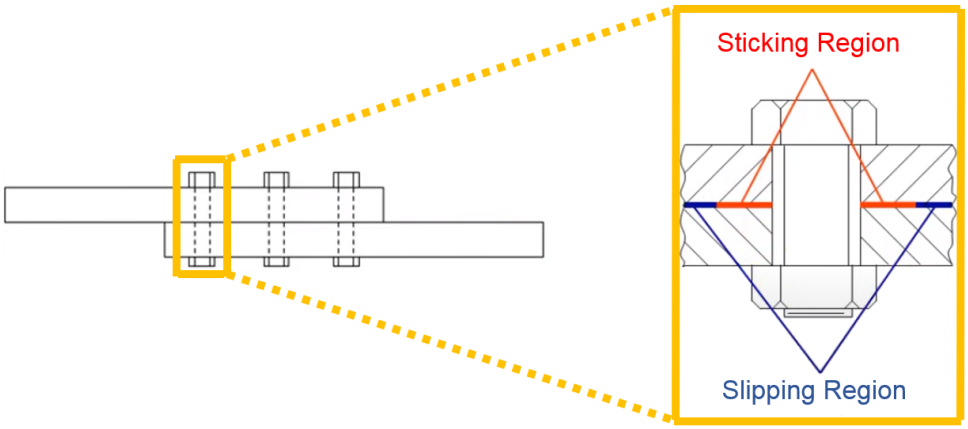

Figure 1.3 Sticking and slipping region within the area of influence of a bolt [8].

In the sticking region the clamping force is large enough to prevent any slip between interlocking asperities. A slipping region surrounds the sticking zone wherein the clamping force is lower. Inside this region the clamping force is in a goldilocks zone: it is not too large to cause asperity locking or too small to cause gross sliding. With a clamping pressure that is just right, the tallest of the asperities in both surfaces will lock in to provide the necessary stiffness, leaving other asperities to be in a state of frictional rubbing that dissipates vibrational energy and hence providing damping. The tenet of the present work is that micro-slip may be enhanced by appropriately texturing the joint interfaces. To this

end, EDM has been used as the texturing process, aspects of which are discussed in the following.

1.3 Electrical discharge machining

EDM is a non-conventional machining process used to machine electrically conductive materials by means of controlled, repeated electrical spark discharges. Unlike conventional machining techniques, EDM is not affected by the workpiece hardness but by its thermal and electrical characteristics. During an EDM process there is no physical contact between the tool and the workpiece, thus there is relatively low mechanical loads applied to either the tool or the workpiece.

In EDM, the electrode and the workpiece are physically separated by a gap across which a pulsed voltage is applied (Figure 1.4a). The gap is filled with a dielectric fluid that is either a hydrocarbon oil or deionized water. Using a servo-controlled feed mechanism the gap is incrementally reduced until it is small enough so that the applied voltage can overcome the breakdown voltage of the dielectric fluid creating a plasma channel (Figure 1.4b). Current flows through the plasma channel generating temperatures high enough to melt and vaporize material from the workpiece and tool leaving a distinct crater behind (Figure 1.4c). The high temperatures achieved during the discharge evaporates some of the dielectric fluid causing a rapid bubble expansion followed by a bubble collapse which helps remove the molten material (Figure 1.4d).

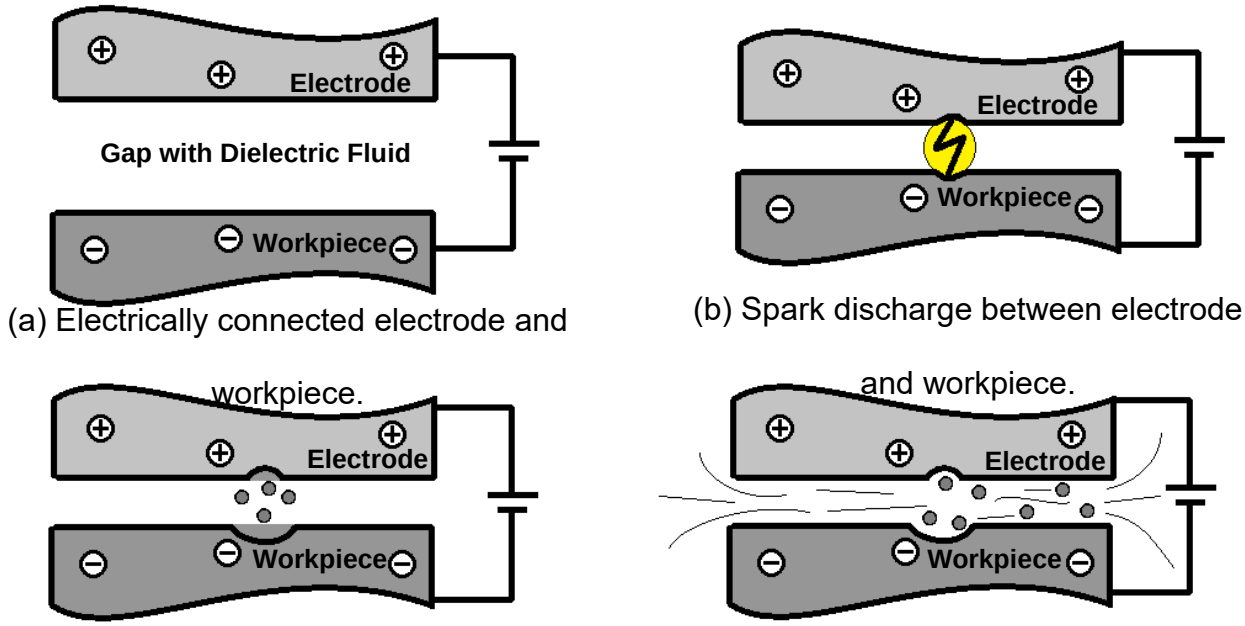

(a) Electrically connected electrode and workpiece.

(b) Spark discharge between electrode and workpiece.

(c) Electrode and workpiece eroded surfaces.

(d) Debris washed away as the dielectric rushes back into the gap.

Figure 1.4 Stages of an EDM cycle.

Such a machining cycle takes just several microseconds. Machining progresses in the frontal area between the tool and the workpiece, with several million sparks that selectively remove material from the workpiece, generating a distinctive surface (Figure 1.5). Surfaces generated using EDM have a height distribution that is positively skewed (Figure 1.6a), which means that the surface comprises relatively few peaks in the midst of a large number of valleys (Figure 1.6b), which are deemed in this research to promote micro-slip induced damping.

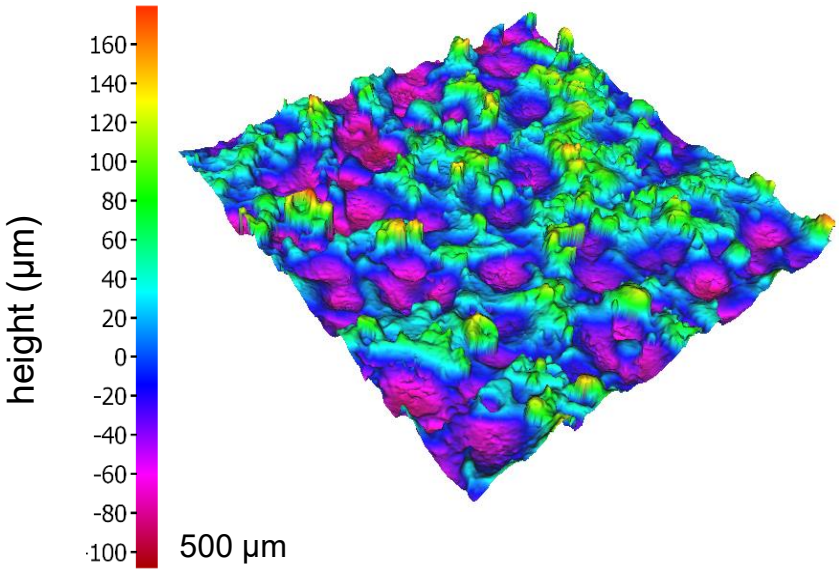

Figure 1.5 EDM-generated surface

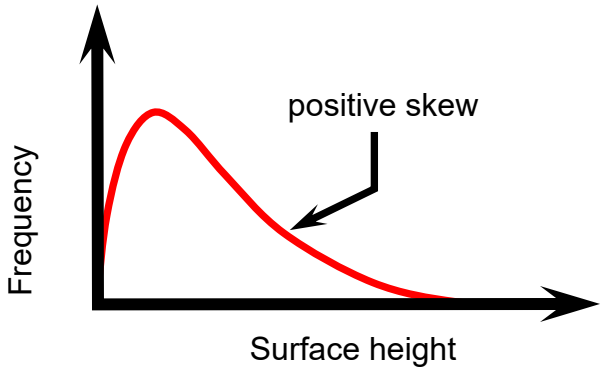

(a) Surface height distribution of an EDM surface.

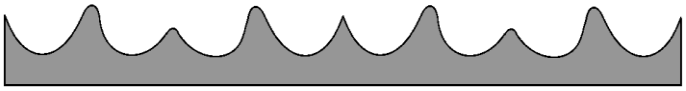

(b) Characteristic EDM surface.

Figure 1.6 Surface height characteristics of an EDM-ed surface.

1.4 Scope of Thesis

In this research a passive damping approach called micro-slip is investigated to increase damping in cutting tools. Micro-slip enhancing textures were eroded using EDM. Textured surfaces were generated by systematically varying EDM parameters such as discharge duration and current, and their damping capability was characterized. This knowledge was then applied to enhance the dynamic performance of a commercial parting tool.

The following chapter presents a comprehensive review of the pertinent literature so as to place the present research in context.

Chapter 2

2 Literature Review

Self-excited vibration known as chatter is a factor that limits productivity in machining operations. Chatter leads to poor surface finish and accuracy and can even cause structural damage to components of the machining system.

A comprehensive review on chatter in milling, turning, and drilling processes, along with chatter suppression techniques including passive and active strategies, have been presented by Munoa *et al.* [9]. Machining stability may be enhanced by moving machining parameters to stable regions, although this may be constrained by workpiece materials with poor machinability. Alternatively, tools specially designed to obstruct self-excitation and promote process damping may be used. Approaches that involve enhancing the stiffness or damping of the system may also be applied to soften the critical mode of vibration.

This chapter provides a brief overview of active and passive vibration suppression techniques in machining, so as to place the present thesis in context. Particular focus will

be placed on passive damping techniques that use friction to dissipate vibrational energy. Studies that investigated the mechanism of frictional damping arising from contacting metallic interfaces will be presented. Lastly, studies that looked specifically at the topographic characteristics of textures that were used to obtain damping will be presented to explain the role of surface asperities in energy dissipation.

2.1 Active Chatter Suppression Techniques

Active damping techniques employ piezoelectric or electromagnetic effects, or smart fluids that respond to electric or magnetic fields. Lu *et al.* [10] presented a system that was used to damp lateral modes of vibration in boring bars to increase the limiting depth of cut. The actuator was a noncontact magnetically activated system that comprised four electromagnets around the boring bar. The setup mounted on a lathe can be seen in Figure 2.1.

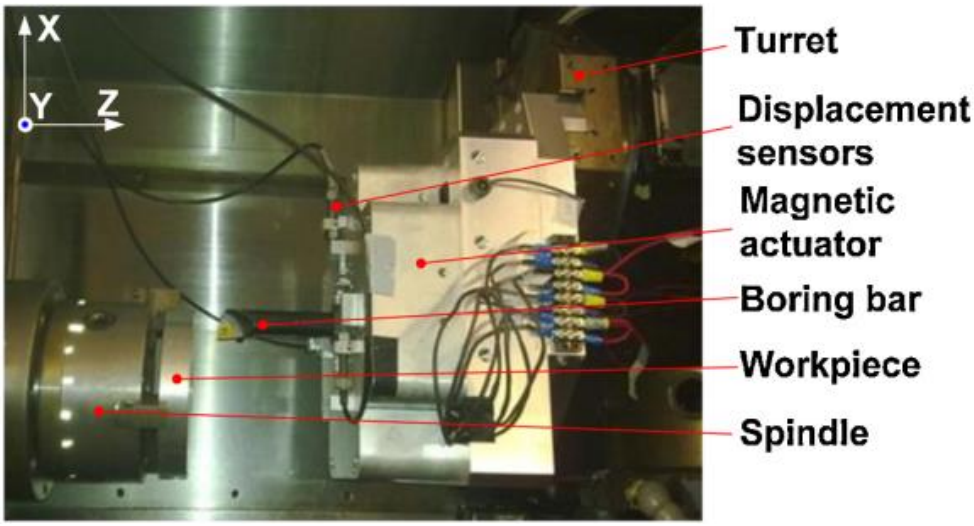

Figure 2.1 Magnetic actuator mounted on lathe turret [10].

Each of the four magnetic actuators had a stator core and an armature core, an actuator housing, one permanent magnet, and two excitation coil windings. Three displacement sensors were used to measure the X, Y and θ displacements encountered by the boring bar while machining. The displacement sensors were linked to a control system in a feedback loop, such that the control would be able to read the displacements and activate the magnetic actuators, moving the armature core to appropriately counteract the motion of the boring bar. The system presented was effective in increasing the dynamic stiffness of the boring bar in two of its major modes of vibration, thus increasing the limiting depth of cut.

Saleh *et al.* [11] created a magnetorheological (MR) fluid damper that was mounted around a boring bar. Using a powerful electromagnet, the fluid viscosity could be altered to increase the stiffness and damping of the system in a semi active manner. This new system consisted of 3 parts: a support structure, a large toroidal shaped electromagnet requiring 0.25 A to operate, and a sponge-like structure to contain the MR fluid (Figure 2.2).

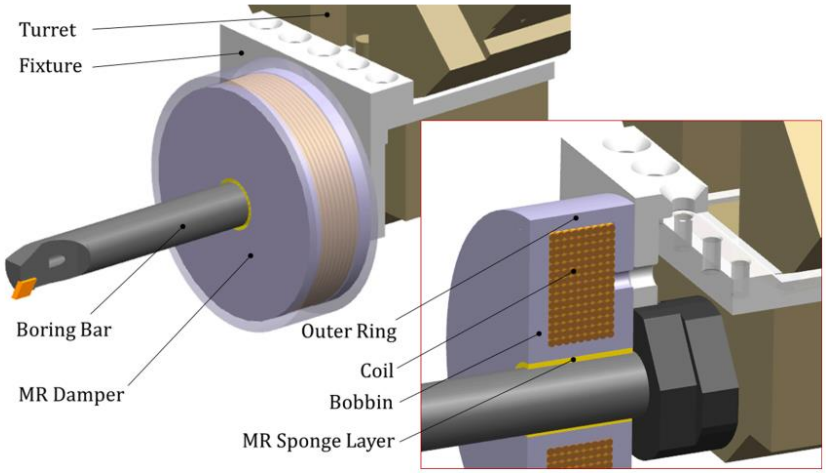

Figure 2.2 CAD model of MR damper mounted on a machine turret [11].

The MR fluid had an anti-sedimentation additive mixed in it, so as to avoid sedimentation of the magnetic particles and thus increase its useful life to 4 months. This MR fluid when activated by the electromagnet was able to increase the system damping and so increase the limiting depth of cut. Active and semi-active damping systems are less effective in suppressing high frequency chatter and are constrained by challenges with actuator sizing and the shifting process dynamics with the progression of material removal.

2.2 Passive Chatter Suppression Techniques

Passive damping approaches have essentially entailed tuned mass dampers (TMD) whose dynamic parameters are adjusted to align their natural frequency with the critical frequency of the vibration that is to be suppressed. Their function is restricted to this target frequency, and it is frequently problematic to physically accommodate them at locations where the modal displacement is large, in order to maximize their effectiveness.

2.2.1 Tuned Mass Dampers

Saffury [4] presented a TMD that could be used in parting and grooving operations. The TMD consisted of two masses linked by a set screw and encapsulated in a rubber O-ring, forming a dynamic vibration absorber (DVA) subsystem. The DVA was mounted to the bottom side of the free end of the parting blade, as illustrated in Figure 2.3. A TMD works by having the mass of the subsystem vibrate in a specific frequency, that

counteracts the motion of the primary system. The positioning of the subsystem is hence crucial to the function of the TMD. This means that the vibrating mass should be able to induce significant deflection in the primary system when it vibrates, otherwise the subsystem will have no significant effect on the overall vibration of the assembly. Thus, to maximize the TMD effectiveness, the DVA must be placed in a region where the primary system is most flexible.

The ingenuity in the TMD from Saffury comes from placing the subsystem in an extension to the body of the main parting blade. Other TMD systems require a cutout in the main body of the parting blade to place the DVA, which reduces the stiffness of the blade. Although it is innovative, the TMD presented by Saffury still suffers from the drawback of all TMD systems that they require tuning, which is specific to the machining application.

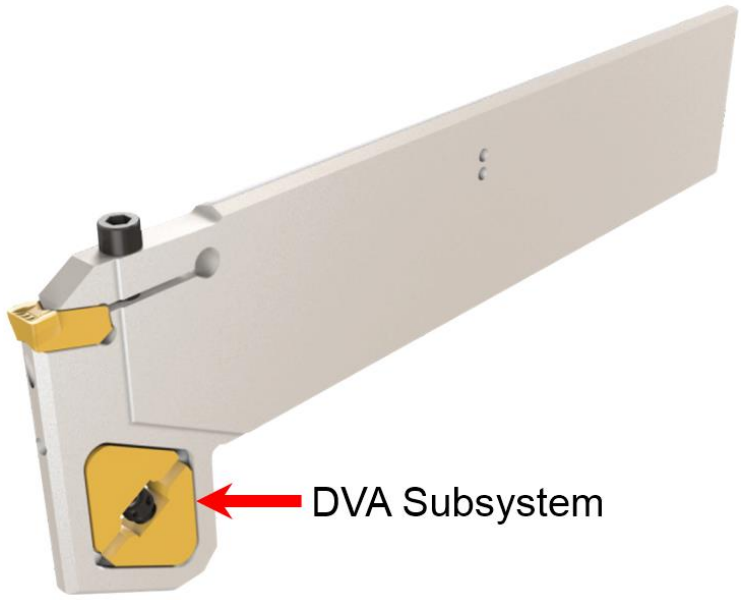

Figure 2.3 DVA mounting in a parting blade [12].

2.2.2 Particle Impact Damping

Some passive techniques focus on the use of frictional forces or the energy loss from particle collisions to damp vibrational motion. These are known as Particle Impact Damping (PID) systems and have been implemented in a wide range of applications including chatter suppression in machining.

Biju *et al.* [13] presented a method for chatter suppression in boring bars that works on this principle which makes use of energy loss that occurs through friction and momentum exchange between colliding masses [2]. Their particle impact damper consisted of a boring bar with a hollow cavity at the free end. The hollowed-out cavity was filled to different volumes with steel spheres of various diameters. Sphere diameters of 3.17, 3.97 and 4.76 mm and cavity fill ratios of 30%, 50% and 70% were investigated. Figure 2.4 shows a hollow boring bar partially filled with steel spheres.

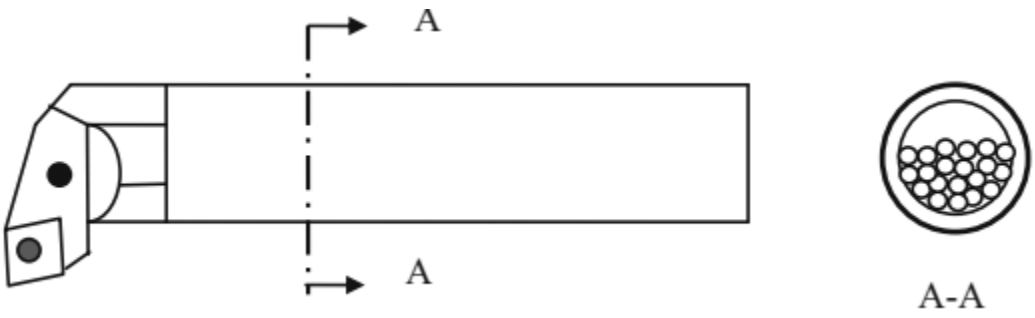

Figure 2.4 Hollow boring bar partially filled with steel spheres [13].

To evaluate the best performing combination of fill ratio and sphere diameter a shaker test was conducted and the tip displacement of the boring bar was compared for every situation, to identify the combination that gave the lowest displacement. The best performing combination had a 50% fill ratio with spheres of 3.17 mm in diameter. This combination was used in boring operations showing a decrease in the roughness of the machined surface by up to three times when comparing to other combinations, and a decrease of 70% when compared to a situation without a PID.

The use of PID systems is not confined only to machining operations; Panossian *et al.* [2] showed the effectives of PID in reducing the amplitude of vibration for critical modes of the space shuttle main engine inlet. To achieve damping of these critical modes, they drilled four 1 mm holes in key points in the engine inlet and filled them with particles of different materials and sizes, while varying the fill ratio in the four cavities. The best situation achieved an amplitude reduction of more than 5 times while increasing the system mass by only 1 gram, which caused an insignificant change to the natural frequency and mode shape of the structure.

Although effective, PID mechanisms are complex to implement, requiring extensive dynamic studies on the structure in order to detect the optimum placement of the cavity and the optimum combination of cavity fill volume and particle mass, without a sound theoretical basis.

2.2.3 Frictional Damping

Frictional energy dissipation is a simple and elegant passive method to achieve damping which uses the friction that occurs in contact interfaces due to vibration-induced relative motion. This is the larger focus of this thesis.

Mauri *et al.* [3] proposed a passive method of damping cantilever-like tools, taking advantage of the micro-slip phenomenon that happens at the interface between two contacting bodies. The proposed system consisted of slotting a rectangular hole in a steel beam and inserting a rectangular block into the machined slot with an interference fit. The whole setup was then clamped to a vice along with two load cells, creating a cantilever structure, as illustrated in Figure 2.5. The position of the rectangular hole was varied by machining it either near the free end or near the clamped end of the beam.

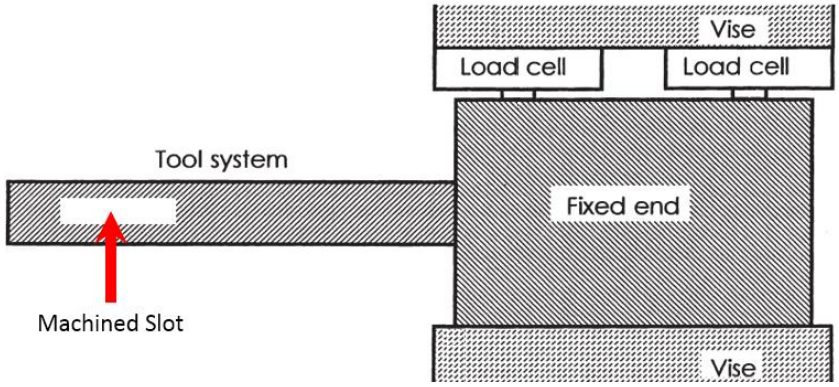

Figure 2.5 Experimental setup clamped on a vise [3].

Clamping forces varying from 6 kN to 20 kN were used in the investigation. Five different interference fits involving 90, 110, 120, 130 and 150 microns were also tested. Combinations involving slot positioning, clamping forces and interferences were tested by means of hammer impact tests on the cantilever beam, to determine the combination that corresponded to the highest damping ratio.

Marui et al. concluded that the optimum slot position was close to the clamped end of the beam, rather than the free end. A similar phenomenon was encountered in the present research, where the damping ratio obtained was also dependent on placement of the textured insert, the reason for which will be discussed later. Mauri and colleagues also found that increasing the clamping force resulted in a decrease in the damping ratio: an increase of 7 kN clamping force led to a decrease of over 50% in the damping ratio. Also, although inserts with a larger interference increased the system stiffness, they corresponded to lower damping ratios.

Ziegert *et al.* [14] presented a different kind of frictional damper, which they named a Centrifugal Damper. This innovative damper used finger-like structures cut from a cylinder that was inserted into a hollowed-out end mill (Figure 2.6). The function of this damper relied on centrifugal forces generated from rotation of the tool during milling, which pushed the finger structures against the inner surface of the drilled hole in the end mill. This combined with tool bending from machining forces gave rise to relative displacement between the finger-like structures and the inner surface of the end mill, thus creating frictional losses.

Such frictional damping was found to more than compensate for the loss in stiffness due to removal of material from the end mill to accommodate the finger structure.

In order to minimize stiffness loss, the researchers made the central hole in the end mill to be one-half of the outer diameter, which resulted in a stiffness loss of only 7%.

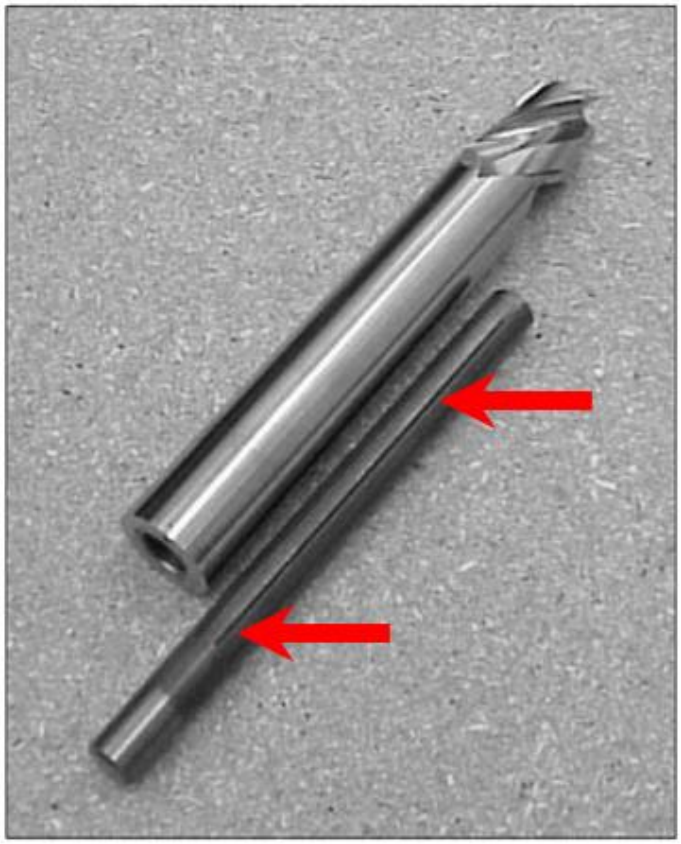

Figure 2.6 Centrifugal damper. Red arrows indicate the finger-like structures [14].

Machining tests were conducted in aluminum blocks for three instances: a hollowed-out end mill, a solid end mill and a hollowed end mill with 8 finger inserts, in order to determine the limiting depth of cut for each situation. The authors found that the damper outperformed a conventional end mill in every spindle speed between 10000 RPM and 23000 RPM, although with varying degrees of success. In the best case, a 53% increase in the limiting depth of cut was achieved.

Hayati *et al.* [15] proposed a new method of frictional damping for boring bars. They drilled longitudinal holes along the length of the boring bar that were radially spaced in the circular cross-section. Steel rods were then press fitted into each of the drilled holes, as illustrated in Figure 2.7.

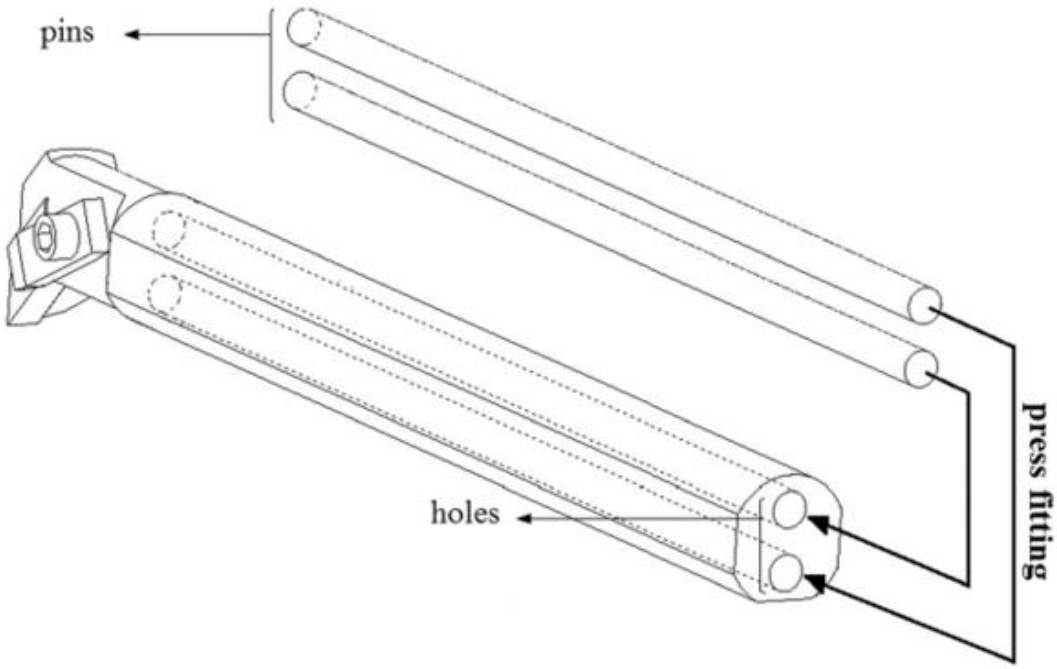

Figure 2.7 Experimental setup for a two-pin configuration [15].

Much like the centrifugal damper created by Ziegert *et al.* [14], this damper takes advantage of the relative motion between the inner walls of the drilled holes and the outer walls of the steel rod inserts to dissipate energy through friction whenever the bar bends in vibration. The researchers evaluated the effect of using different interference fits for the steel rods as well as the number of inserted rods.

Finite element analyses were carried out for interference fits of 6, 7, 8 and 9 microns in combination with setup configurations with 2, 3, 4 and 5 inserted rods. From analyzing the FEA results, Hayati and colleagues concluded that smaller values of interference fits led to better performing boring bars, similar to the findings by Mauri *et al.* [3]. The FEA analysis further showed that increasing the number of inserted rods led to better performing boring bars, pointing to the possibility that the energy dissipated by rubbing contacts is influenced by the contact area at the interface.

A boring bar that is 25 mm in diameter and 282 mm in length was drilled by Hayati et al. using sink electro discharge machining (EDM) and subsequently steel pins were press fitted in order to construct a real model of the best performing arrangement obtained through FEA. Although not investigated by the researchers, the holes were made by EDM likely due to requirements referring to close tolerances and high aspect ratio holes, seemingly unaware that the EDM process itself has an influence on the damping obtained, as will be shown in this thesis. To validate the FEA results and compare the performance of the constructed boring bar to a commercial one, the researchers ran tap tests on the bar, capturing the frequency response function (FRF) and extracting the modal parameters for the most flexible mode of vibration. This showed an improvement of 37% in the damping ratio for the most flexible mode of vibration when compared with a commercial boring bar.

In the papers presented above, the nuances of frictional damping in the context of the interfaces themselves were not considered in detail. The following presents a brief review of such characteristics of frictional damping in metallic interfaces.

2.3 Frictional Damping in Metallic Contacts

Analysis of bolted joints and such loaded metallic contacts allows for a better understanding of frictional damping. Some of the parameters of influence are reviewed in the following.

2.3.1 Effects of Joint Characteristics

Rogers *et al.* [16] studied the effect of damping on metallic interfaces in the regime before gross slip was initiated. They varied the metals in contact at the joining interface under a normal load, applied loads tangential to the contact plane and measured the energy loss caused by rubbing between the metallic surfaces.

The experimental setup consisted of a metallic cup-shaped structure covered by a lid that was able to slide over the cup (Fig. 2.8). The setup was firmly attached to a steel table. The lid was preloaded with dead weights allowing for variations in the contact pressure and forming an annular-shaped contact area with the cup underneath. The researchers varied the lid material: grey cast iron, low carbon steel, brass and 2024-T4 aluminum, to investigate the effect of the material contact pair. All the lids used were ground flat and subsequently lapped, creating a texture that had either perpendicular or parallel machining lays.

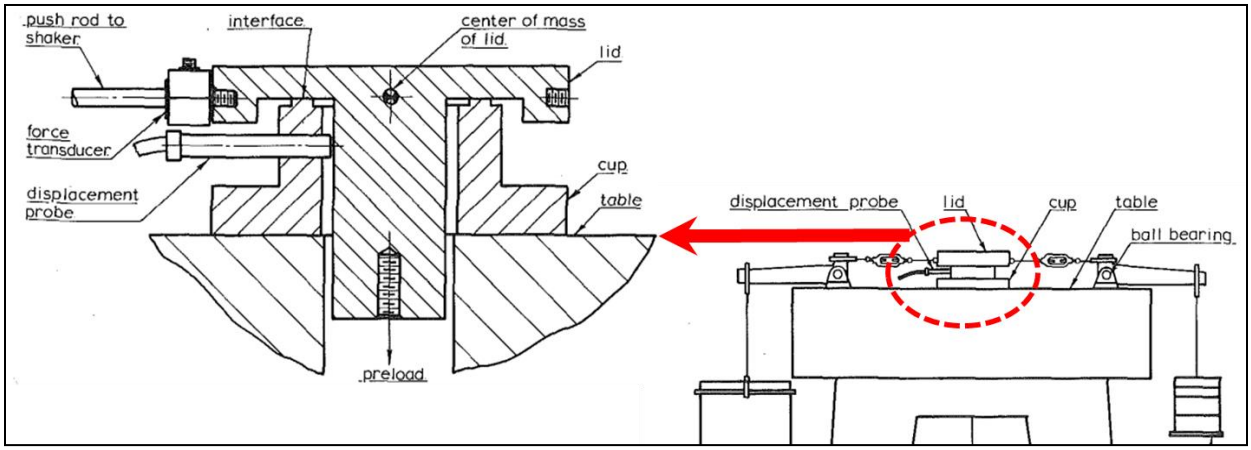

Figure 2.8 Cup and lid setup for evaluating frictional damping [16].

After applying different normal loads to the contact pairs and measuring the lid displacement for specific tangential loads, hysteresis loops were plotted. A comparison of the energy dissipation per cycle of various materials can be seem in Figure 2.9. The lid material that had the most energy dissipation was aluminum. When evaluating the effects of contact stiffness, lid material, normal load and coefficient of friction on the energy loss per cycle, the researchers found an exponential relationship between the coefficient of friction and the energy loss per cycle. In order to maximize the energy loss per cycle in the microslip regime, they concluded that it is desirable to have a high coefficient of friction, a low contact stiffness and to reduce the normal load at the contact interface such that it is just below the threshold that causes gross slip.

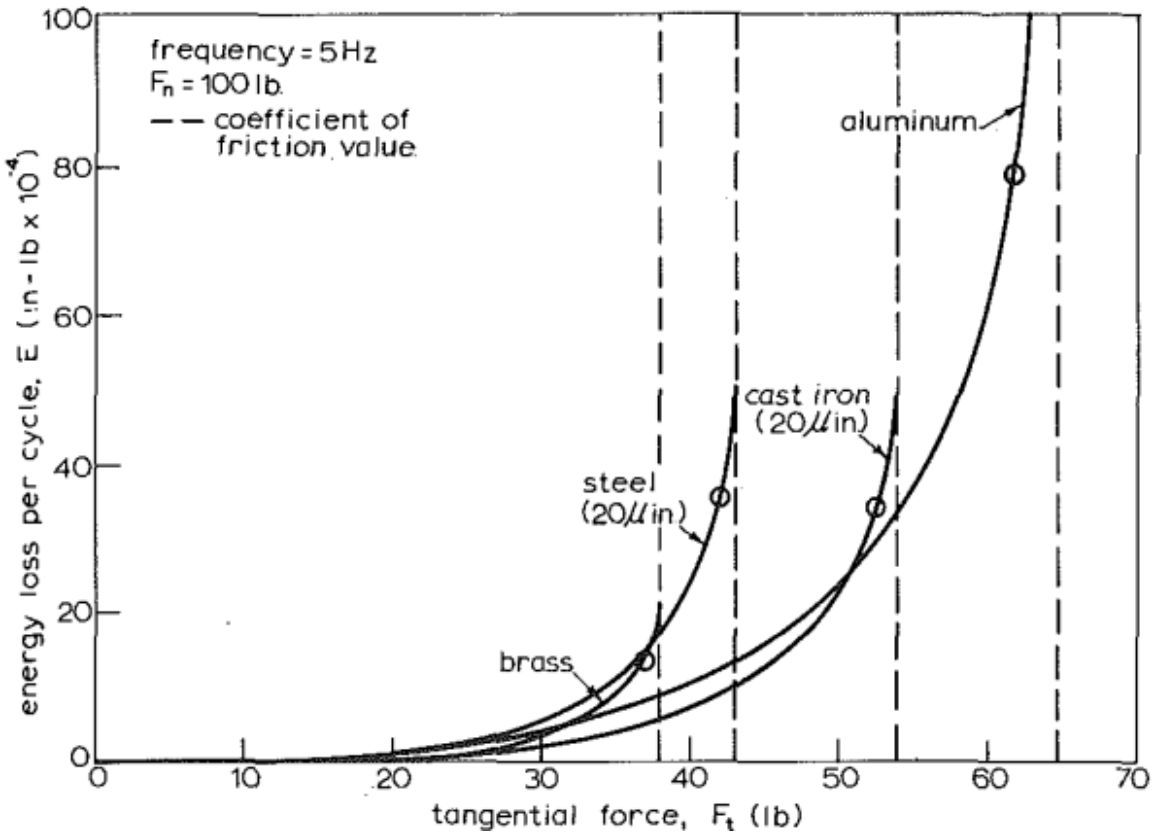

Figure 2.9 Energy loss per cycle for different metallic contact pairs [16].

Mauri *et al.* [17] investigated the effects of surface topography by creating different surface textures on the contacting interfaces of metallic joints. They looked at the effect of adding non-metallic materials in the interface and adding an interface with milled 0.64 mm tall pyramid-like structures on both contacting surfaces, as well as mixing both of these. They created their experimental setup by clamping a long thin plate alongside two shims and two load cells in a regular vice (Figure 2.10). The shims were placed one on each side of the long thin plate and the load cells were placed side by side against the movable jaw of the vice. To evaluate each of the tested situations they extracted damping ratio values from the most flexible mode of vibration in every tested situation and

compared it with the damping ratio obtained from a control experiment that referred to only the shims and the thin plate clamped in the vice.

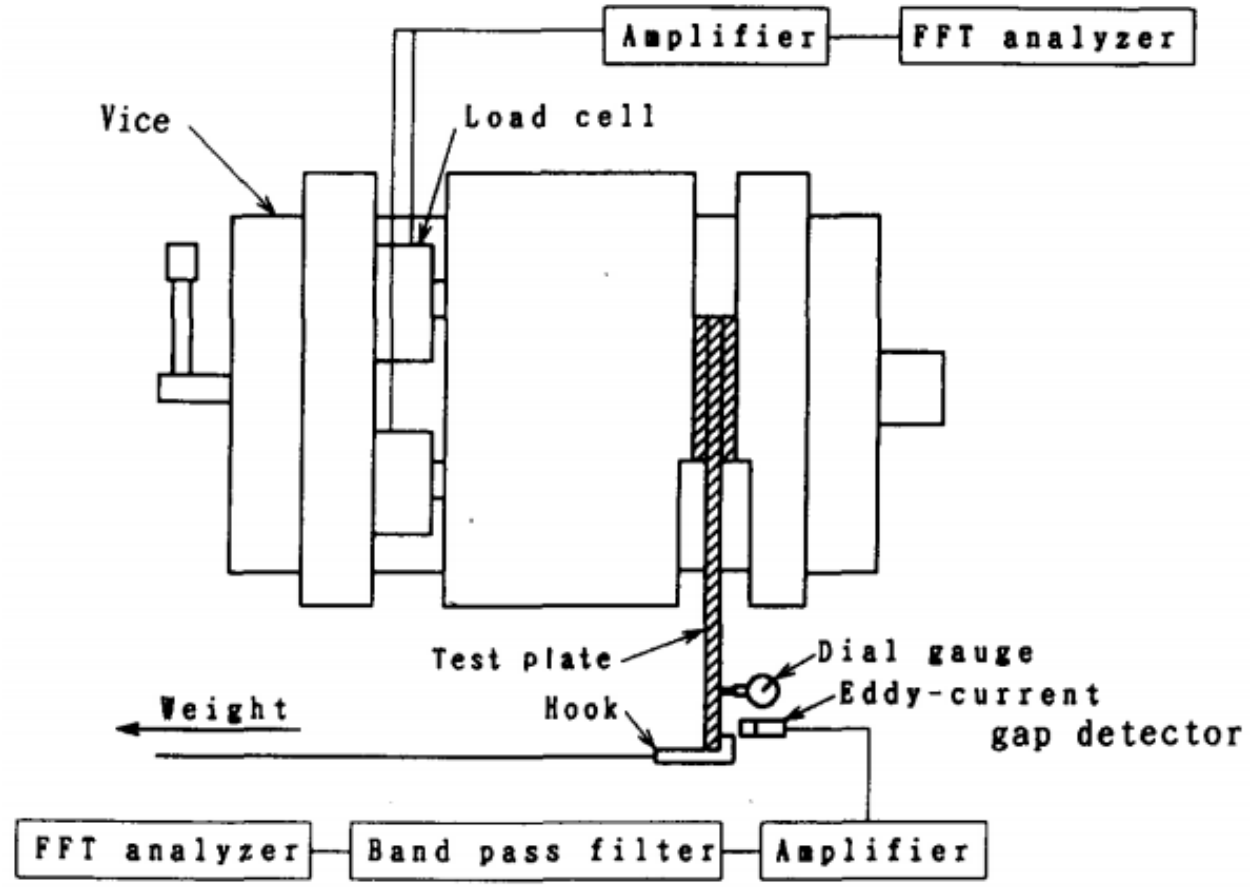

Figure 2.10 Thin plate clamped on a vice with two shims and two load cells [17].

Mauri et al investigated four contact situations. In the first one, they created a sandwich structure composed of piano wires and adhesive tape, then they placed the composite in the contact interface between the shims and the thin blade. The second situation consisted of milling pyramid-shaped projections on the contacting surfaces, generating a surface pattern like the one illustrated in Figure 2.11. For the third situation the researchers used epoxy resin to bond the shims to the thin plate. Finally, in the fourth

situation adhesive tape was used to create a less permanent contact between the shims and the long thin plate.

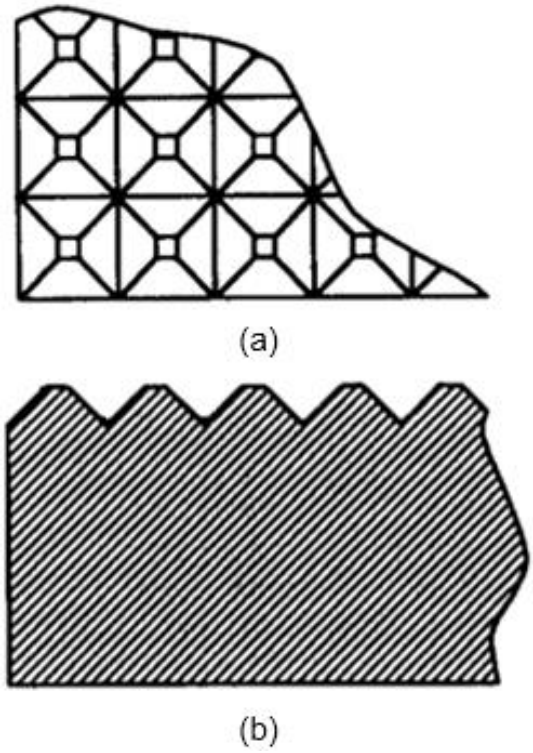

Figure 2.11 a) Top view of milled pyramid-shaped pattern. b) Side cross-section view of pyramid-shaped pattern [17].

From their results the researchers were able to conclude that for almost every situation, the static stiffness of the setup was inversely proportional to the damping ratio. This was most noticeable when evaluating the epoxy bonded contact. For this specific situation the static stiffness obtained was approximately 50% higher than the control, while the extracted damping ratio decreased by half. The milled pyramid structure was the only configuration capable of maintaining stiffness comparable to the control arrangement, while delivering a 100% increase in the damping ratio.

In addition to the materials that form the contacting interface in controlling microslip, another import parameter is the pressure distribution in the contact region [3][15][16], as discussed in the following.

2.3.2 Effect of Contact Pressure Distribution

Investigating the effect of surface pressure distribution, Wentzel *et al.* [18] studied how manipulating the contact pressure on the joining interface would influence damping in bolted structures. The researchers inserted thin metal sheets with cutouts into bolted lap joints, and by varying the cutout shapes, they changed the contact pressure distribution in the joint.

For their experimental setup the researchers used a simple lap joint connected by two bolts (Figure 2.12). In their experiments they maintained constant insert size and bolt tightening torque, ensuring that any change in pressure distribution comes from the insert cutout pattern.

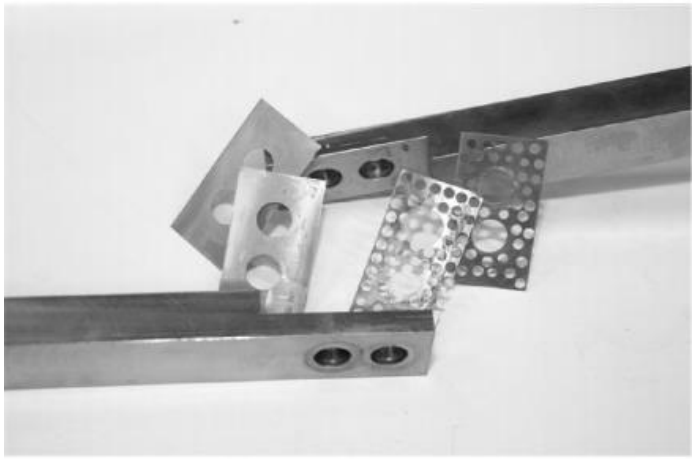

Figure 2.12 Lap joint setup and two of the evaluated samples [18].

Out of all the cutout geometries tested, from drilling an array of holes, to cutting out slots, three cutout patterns were of particular interest. These are depicted in Figure 2.13 a, b and c. The pattern in Figure 2.13a consisted of a cutout slot that reduced the insert thickness at the white region. The insert in Figure 2.13b was used as a control, thus it had no pattern. Figure 2.13c shows an insert pattern composed of drilled through holes, indicated by the white circles. The pattern in Figure 2.13a was the worst, and the one in Figure 2.13c was the best, relative to the control in Figure 2.13b. This highlighted the importance of pressure distribution at the contacting interface in altering energy dissipation per cycle in a bolted structure.

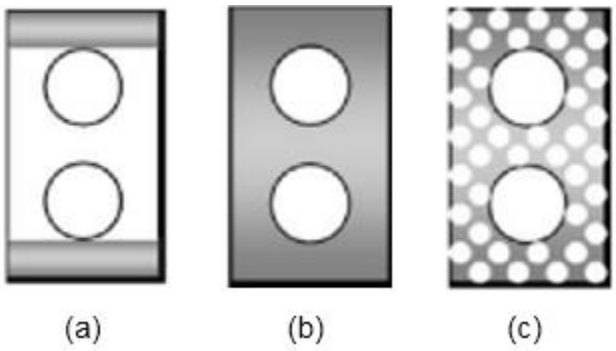

Figure 2.13 Cutout patterns that showed the maximum influence [18].

From analyzing their results, the authors also showed that larger amplitudes increased the energy dissipation per cycle. Furthermore, from comparing the three selected patterns at the same amplitude of motion, the authors calculated an approximately 100% increase in the energy loss per cycle, between the worst case and the best case, and a 60% increase when comparing the best case against the control.

2.3.3 Effects of Surface Topographic Characteristics

The research conducted by Medina *et al.* [19] that involved numerical simulations show a relationship between the topographic characteristics of a surface texture and the damping ratio achieved by that texture. They investigated how texture characteristics like roughness, skewness and kurtosis can increase the energy dissipation of contacting interfaces.

In order to execute their study, the authors created a mathematical model of the contact region between a sphere and a plane, covering this contact area on both objects with a grid. Then, for each point on the grid a correlative point on the opposite object was specified, thus allowing the authors to model the stick and slip behavior on the whole contact area in a point-by-point basis. To model a surface texture on the contact region the researchers generated a gaussian distribution representing a surface height distribution for an artificial texture. They then applied the artificial texture to both contacting objects. This approach allowed them to create textures with any skewness, kurtosis or roughness values, by manipulating the distribution parameters.

The results obtained by Medina et al. allowed for the visualization of how energy dissipation takes place at a contact region under microslip. The researchers plotted the location of each grid point and color coded the points in relation to how much energy they dissipated; this painted a region of energy dissipation. This region was annular in shape, indicating that the contact point was divided in two parts. One part in the center where

there was no energy dissipation and the other part enveloping the center region where all the energy dissipation occurred. Following the same procedure for plotting the pressure distribution and the relative displacement, gave the same annular shape (Figure 2.14 a, b, c).

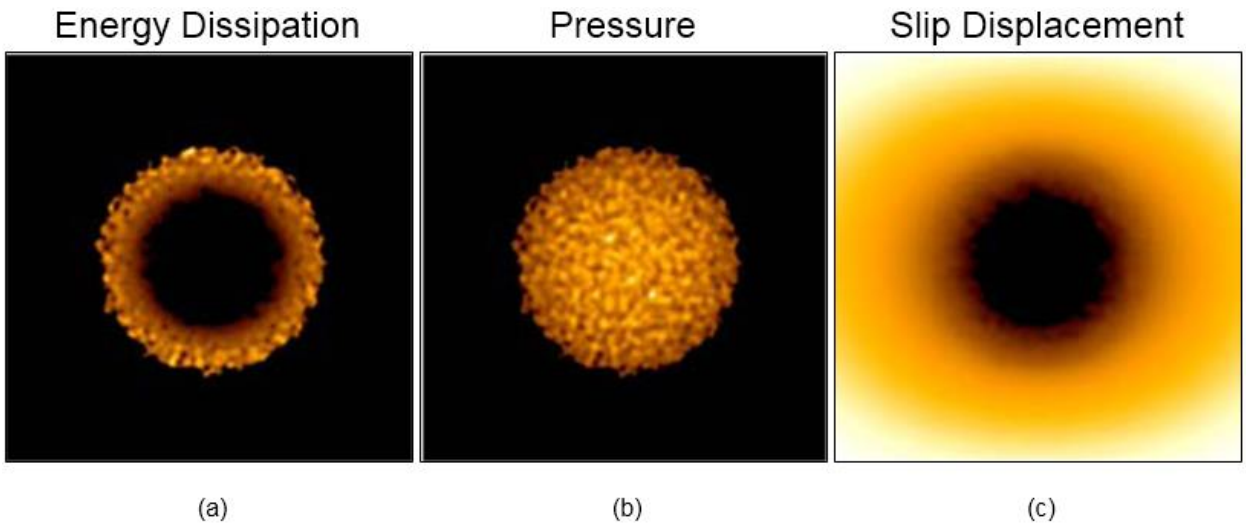

Figure 2.14 a) Energy Distribution at the contact point. b) Pressure Distribution on the contact point. c) Slip Displacement on the contact point [19].

The shape similarity between these graphs indicates the existence of a centered circular region, where all contacting points are in a sticking regime, and a surrounding annular shaped region, where all points are in a of microslip regime. Other works have reached similar conclusions, dividing the contact area into two distinct regions [5][6]. Medina *et al* also found a strong positive correlation between kurtosis and skewness values for a specific texture and the amount of energy dissipation achievable by the texture. This result is shown in Figure 2.13, where red colors indicate a higher energy

dissipation and blue colors a low energy dissipation. This indicates damping to increase with kurtosis, for positively skewed surfaces.

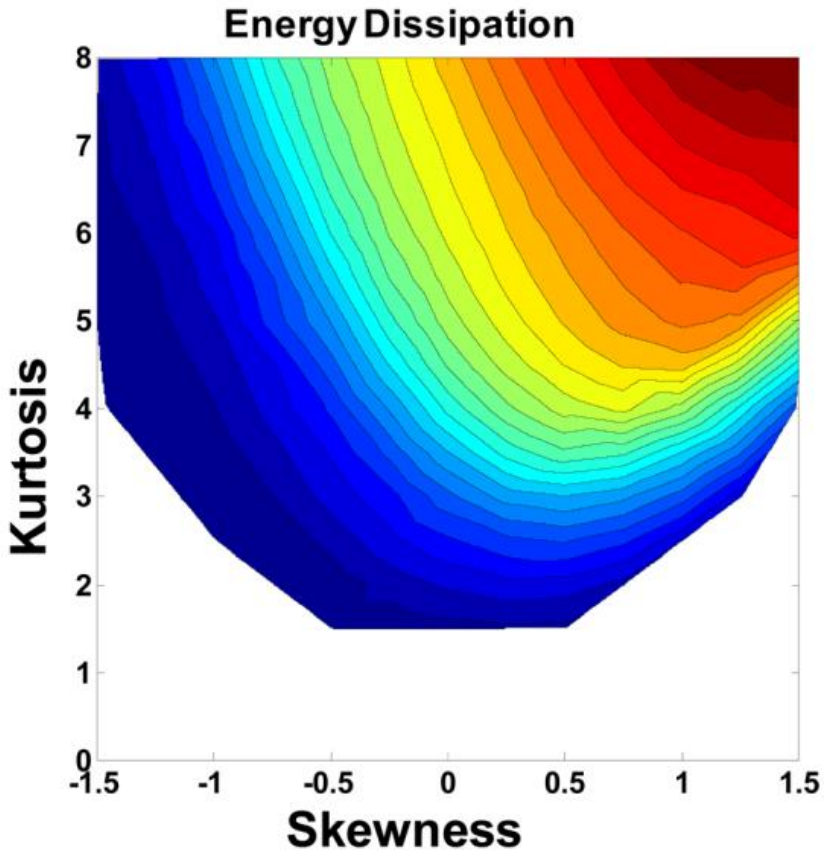

Figure 2.15 Effect of skewness and kurtosis on energy dissipation [19].

The relationship between surface kurtosis, skewness and energy dissipation pointed EDM as a favorable process for achieving surface textures with high damping performance, since EDM is one of the few machining processes capable of generating isotropic surfaces with a positive skewness (Figure 2.16).

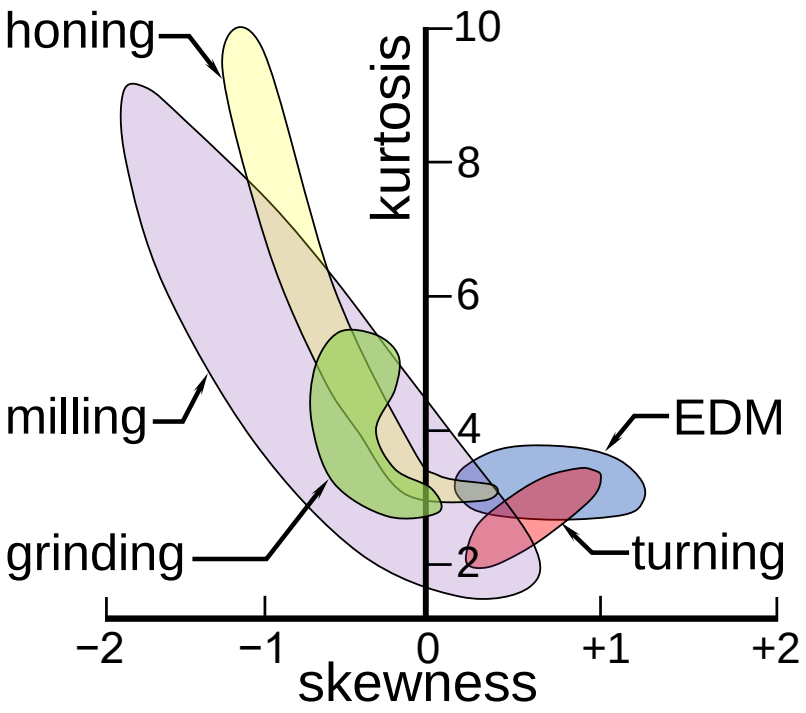

Figure 2.16 Skewness and kurtosis achievable by various machining processes [20].

2.3.4 Prior work on damping from EDM surfaces

An extensive literature search has indicated the work of Beards and Neroutsopoulos [21] to be the only research to use EDM textures as means of enhancing frictional damping. Their investigation does not dwell on the mechanism of energy dissipation or the parameters that affected microslip. Their work focused on just three surfaces of different *Ra* roughness obtained by changing only the discharge current in EDM. It did however show evidence of the robustness of using EDM process. They also found the EDM texture to correspond to a lower fretting damage relative to ground surfaces.

The experimental setup used by Beards and Neroutsopoulos consisted of a steel beam fixed to a large steel block by means of two bolts, creating a cantilever structure that was firmly mounted to a vibration isolated table (Figure 2.17).

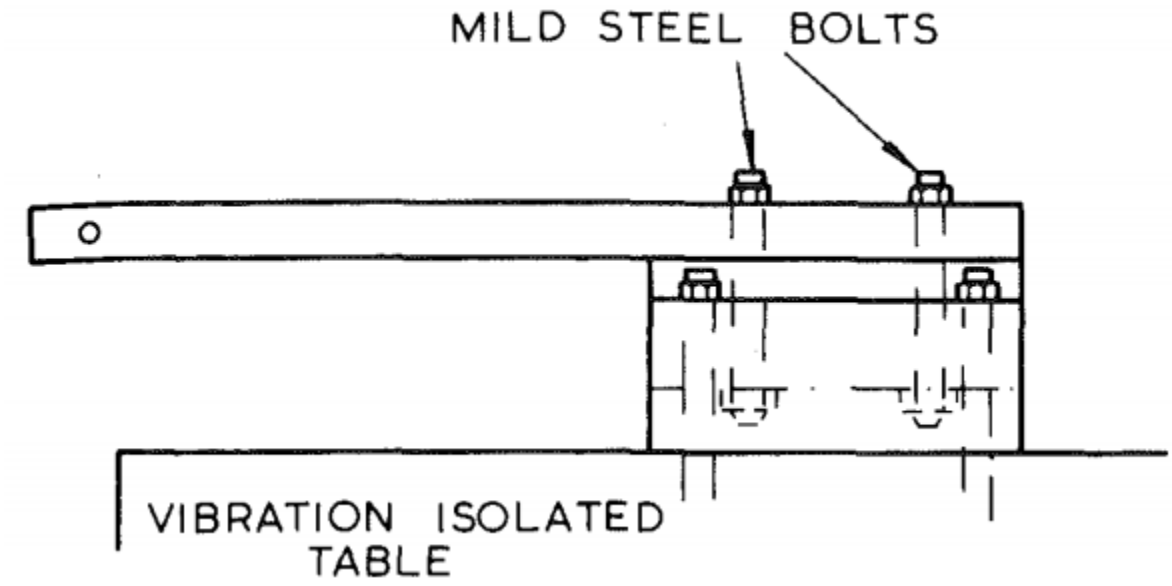

Figure 2.17 Cantilever beam and base mounted to a vibration isolated table [21].

The researchers kept track of the tensioning torque on the bolts so they could analyze how the contact pressure on the interface would affect the static stiffness of the structure. This enabled them to evaluate the minimum static stiffness that would be sacrificed in order to achieve measurable damping values. To determine this value the authors first firmly tightened the structure, then followed by incrementally reducing the tightening torque. The author determined that a static stiffness loss of 10% was necessary to achieve measurable damping values. With this the authors decided to keep the joint mean pressure at 5.5 MPa. Subsequently the contact region between the steel block and the steel beam was textured with three different textures and a shaker test was conducted on the experimental setup. The shaker test ran for a total of 10^7 cycles for each situation, with

inspection intervals at every 1, 3, 6 and 10 x 10^7 cycles. In those inspection intervals, the contacting surfaces were cleaned and inspected for fretting damage, using a microscope and a profile tracer. The loss factor for each situation was extracted from the most flexible mode of vibration and compared with a control situation, were the contact area between the cantilever and the steel block had a ground texture.

Their results showed a 100% increase in the damping ratio when comparing the best of the three textures against the ground surface. The damping values they obtained as a function of the number of cycles is shown in Figure 2.18.

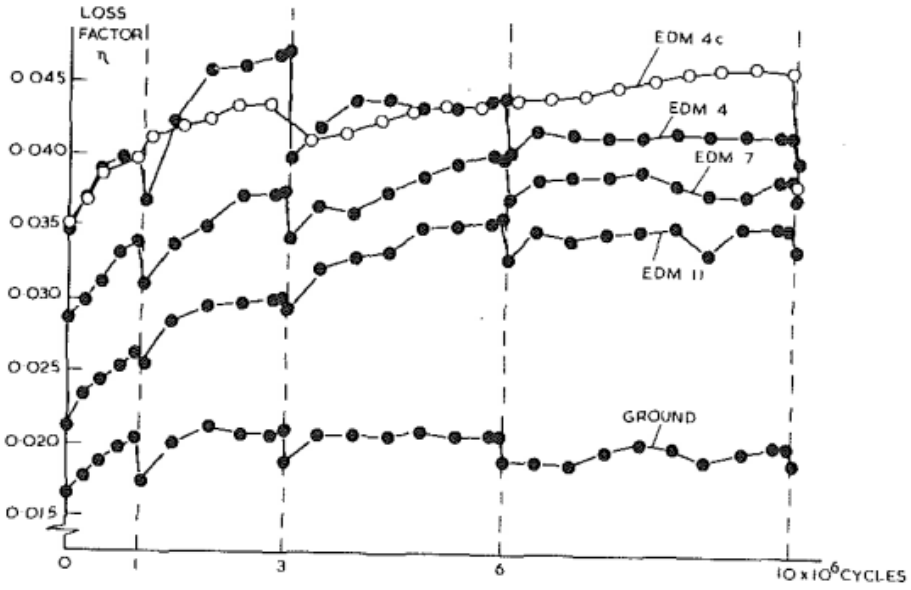

Figure 2.18 Loss factor as a function of number of cycles [21].

From analyzing their fretting damage results, the researchers concluded that after 10^7 cycles, the worst EDM texture had a damaged area of approximately 30 mm^2 and the ground surface pair had a damaged area of over 80 mm^2, meaning the EDM texture generated a 62.5% smaller damaged area. Making the same comparison between the least fretted EDM texture and the ground texture reveals a damaged area that is over

90% smaller. These results show that EDM textures can be used to enhance damping in bolted connections while enhancing fretting resistance by more than 90%.

2.4 Summary

From the review of various damping methods presented in this chapter, frictional damping appears to be a simple and elegant passive method to achieve damping by using the friction that occurs in contact interfaces to dissipate energy.

In contrast to active techniques, frictional damping does not require an elaborate setup, a complicated control system or any external energy to operate. In comparison with other passive techniques, frictional damping does not require tuning, or any structural modification such as drilling holes. Frictional damping can also be used in other areas that are relevant to increase damping in machining, for instance it can be used to increase damping in bolted connections in the machine, and is not confined to regions around the cutting tool.

In this research aluminum inserts were textured by means of electro discharge machining and placed in contact with various interfaces that form the connection between the cutting tool and the machine tool. The influence of discharge current and discharge duration was systematically investigated. Surface analyzes were carried out on the eroded textures to understand the effect of surface characteristics on the mechanism behind energy loss through frictional forces. Subsequently, this knowledge was used to further enhance the capabilities of the eroded textures. Finally, grooving experiments were conducted to show the effectiveness and applicability of the proposed technology.

This knowledge thus represents a significant advance over the work of Beards and Neroutsopoulos [21], which is the only work available on the damping capacity of EDM surfaces, as already alluded to.

Chapter 3

3 Experimental

3.1 Objectives and Methodology

Experiments conducted during this research were accomplished in 2 phases.

Phase I pertained to understanding the damping characteristics of EDM textures. The first section of this chapter will discuss EDM for fabricating textures to evaluate the effect of parameters such as discharge duration and current to maximize damping. This will be followed by a description of the equipment used to characterize the textured surfaces, and the equipment and procedure used to extract the damping ratio from instrumented impact hammer tests using a simple vibrating beam.

Phase II referred to the application of the knowledge gained from Phase I in enhancing the dynamic performance of a grooving tool. In this section the method used for obtaining the stability limit diagram for a grooving tool will be explained, in addition to the setup and procedure used during the grooving experiments.

3.2 Texture Fabrication

The machine tool used for surface texturing was an AGIETRON Impact 2 Sink EDM shown in Figure 3.1. An Intelligent Power Generator (IPG) provides a current ranging from 1.2 A to 72 A and a discharge duration ranging from values smaller than 12 μs to values greater than 2400 μs. Hydrocarbon oil was used as the dielectric fluid, and jump flushing was adopted.

Figure 3.1 AGIETRON Impact 2 Sink EDM machine tool.

Textures were fabricated using copper electrodes by systematically changing the discharge duration from 65 µs to 1200 µs and the pulse current from 21 A to 72 A, to study their effects on the damping characteristics of the eroded surfaces. The workpiece material used was Aluminum 6061, with an erosion depth of 0.5 mm. The textured surfaces were characterized in terms of their *Sa* roughness, skewness and kurtosis using a confocal microscope, the details which follow.

3.3 Surface Topography Characterization

Non-contact surface characterization was done using the Alicona InfiniteFocus G5 (Figure 3.2), a white light interferometer capable of analyzing 3-dimensional surface structures. The instrument has a maximum resolution of 9 nm, and a maximum measurable slope of 87˚. A textured area of 1.62 mm x 1.62 mm was scanned by the microscope in order to conduct the analysis. *Sa* roughness, skewness and kurtosis were then obtained from each scanned surface.

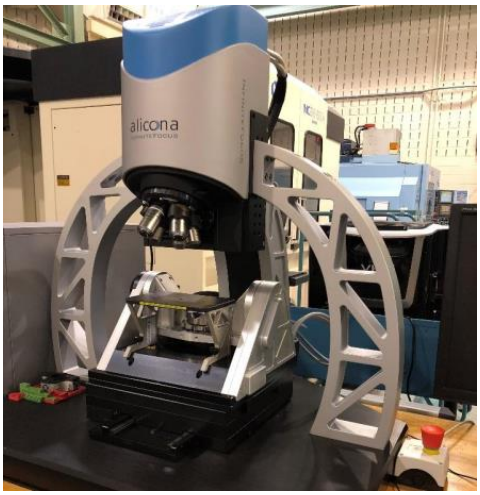

Figure 3.2 Alicona Confocal Microscope.

The textured aluminum pieces were then placed in an experimental setup to determine their damping characteristics through tap tests; this experimental setup will be described in the next section and the tap test procedure in the subsequent section.

3.4 Damping Characterization

In this part of the research textured surfaces were characterized in terms of their damping performance, using a simple cantilever structure. The damping ratio was measured from tap tests using the half-power method. The procedures and materials used will be described in the subsequent sections.

3.4.1 Experimental Setup

The setup shown in Figure 3.3 was used to characterize damping. The setup consisted of a steel beam that had 20 mm x 50 mm in section and 300 mm in length. The textured aluminum pieces were 25 mm in width and 5 mm thick, with a baseline length of 85 mm. The textured aluminum pieces were positioned either on the top, bottom or both top and bottom of the steel beam, as shown in Figure 3.3. Two M8 bolts were used in conjunction with the 3 sets of nuts to clamp the setup to the EDM table as well as to clamp the textured inserts to the steel beam. The bottom most set of nuts in Figure 3.3 were firmly tightened against the table in order to hold the setup in place. The topmost set of nuts seem in Figure 3.3 were tightened with a baseline torque of 11 Nm using a mechanical torque wrench. This tightening torque was chosen based on [21]. The top steel plate was used

both to distribute the clamping pressure from the top nuts evenly to the aluminum top insert, as well as to prevent the aluminum insert from being deformed by the tightened steel nut.

A unidirectional accelerometer was mounted on the free end of the beam to measure the time response of the beam to an impact excitation (Figure 3.4). The accelerometer and the impact hammer were used to perform tap tests on the assembly. The procedure and equipment used for these tap tests will be discussed in the next section.

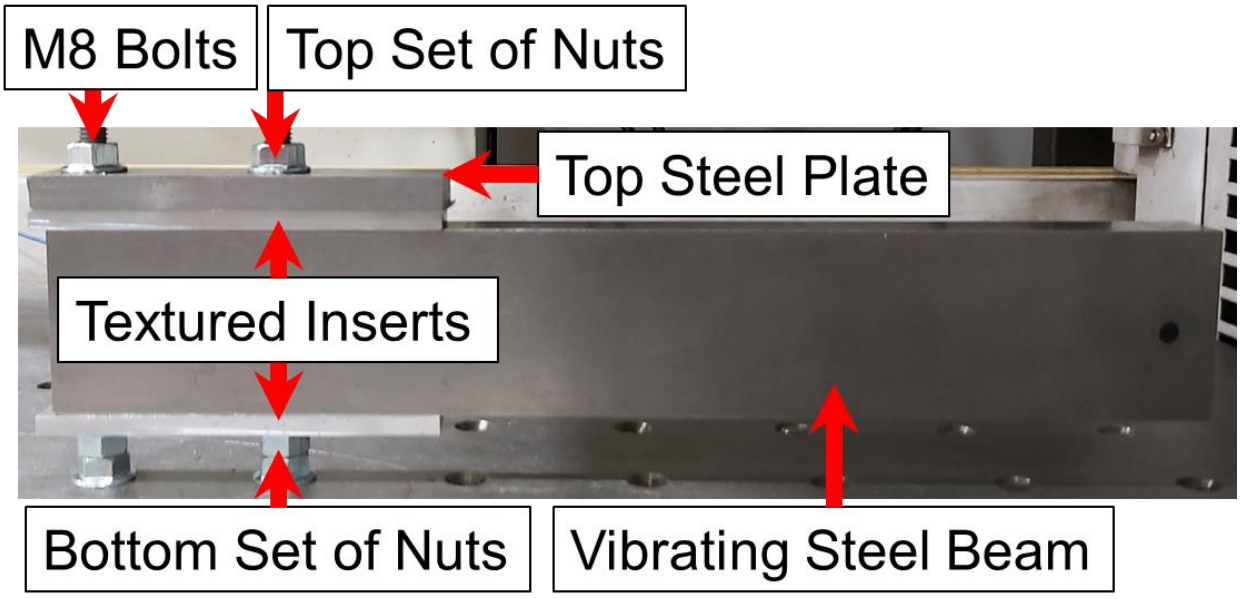

Figure 3.3 Experimental setup for texture characterization.

3.4.2 Tap Tests

For the tap tests a PCB impact hammer model 086C01 along with a Kistler shear type accelerometer model 8702B500M5 were used to capture the impact force and the vibration response, respectively. The hammer had a peak measurement range of ± 444 N and a resonating frequency ≥ 15 kHz. A steel tip was used for the hammer impacts to ensure excitation in the frequency range from 100 Hz to 5000 Hz. The accelerometer used had a peak acceleration range of ± 1,000 g, a resonant frequency ≥ 73 kHz and a useful frequency measurement range of 1 Hz to 10 kHz (± 5%). The data acquired from the sensors was transferred to a computer using a National Instruments data acquisition module NI-9234 connected to the computer via a USB port; the sampling frequency used was 51 kHz. The acquired data was read from the acquisition module with CutPro software developed in the Manufacturing Automation Laboratory at the University of British Columbia.

To perform the tap tests, hammer impacts were applied at the free end of the steel beam, along the X direction, as shown in Figure 3.4. Every tap test result consisted of a total of 5 hammer hits. For every hammer hit one acceleration and one impact signal were captured. After the 5 hammer hits, all 5 acceleration signals were averaged out, the same was done with the impact signals. The final result for one tap test was then the averaged acceleration signal and the averaged impact signal from the five hammer hits.

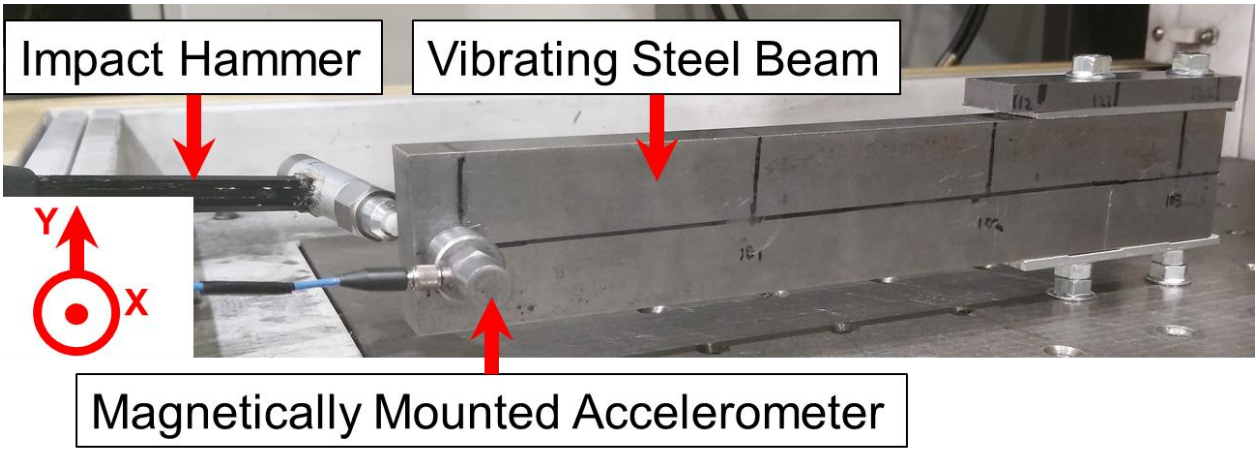

Figure 3.4 Tap test experimental setup.

The striking force was ensured to be within 150 N to 180 N, considering that damping from microslip is amplitude dependent. In consideration of the readings from the accelerometer and the hammer, a direct accelerance frequency response function (FRF) in the XX direction was calculated using CutPro. The real and imaginary parts of these accelerances were then converted to real (R_c) and imaginary (Im_c) compliances using equations 3.1 and 3.2 where $R_{ac}(f)$ and $Im_{ac}(f)$ are the values for the real and imaginary parts of the accelerance at a frequency (f).

$$R_c = R_{ac}(f) \cdot [-\frac{1}{(f \cdot 2 \cdot \pi)^2}] \tag{3.1}$$

$$Im_c = Im_{ac}(f) \cdot [-\frac{1}{(f \cdot 2 \cdot \pi)^2}] \tag{3.2}$$

The real (R_c) and imaginary (Im_c) parts were used in equation 3.3 to calculate the magnitude (Mag_c) of the compliance FRF.

$$Mag_c = \sqrt{R_c^2 + Im_c^2} \tag{3.3}$$

From the magnitude FRF the damping value of the most flexible mode of vibration was extracted, as this is the mode of vibration that exerts the most influence on the dynamic stability of the system. The damping ratio extraction was done using the half power method, as shown in Figure 3.5. This consists of determining the maximum amplitude (*A*) of the FRF at the targeted mode of vibration, along with the mode natural frequency *(f_n)*, using equation 3.4 to calculate the amplitude (A_y) and determining the frequency values for that amplitude for both sides of the FRF curve *(f_1, f_2)*.

$$A_y = \frac{A}{\sqrt{2}} \tag{3.4}$$

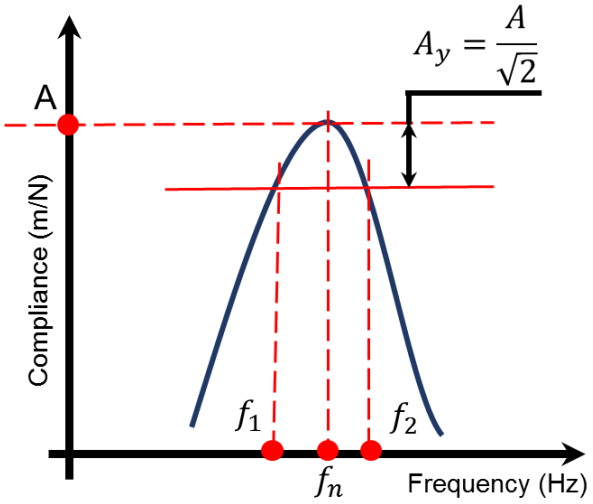

Figure 3.5 Half power method for damping calculation.

With these frequency values extracted, equation 3.5 was used to determine the damping ratio ζ.

$$\zeta = \frac{(f_2 - f_1)}{2f_n} \tag{3.5}$$

The damping ratio (ζ) is a measurement of how close a mode of vibration is to a critically damped state, where a value of 1.0 means that the mode is critically damped, thus it would only oscillate when in a forced vibration state. The damping ratio is normally expressed as a percentage where 100% indicates a critically damped mode of vibration.

The next section will focus on the experimental setup and methods used for evaluating how the surfaces with the highest damping values would perform in a grooving experimental setup, in terms of increasing the limiting width of cut of a commercial tool.

3.5 Grooving Experiment

After determining the best performing textures in terms of damping ratio, the next step was to mount textured inserts in a grooving experimental setup, to determine how much they would improve on the limiting width of cut, and finally machine grooves using the appropriate cutting widths to validate the stability limit diagram calculated. In this section the grooving experimental setup will be discussed, as well as the method used to

calculate the limiting width of cut, followed by the parameters and equipment used during the grooving operation.

3.5.1 Grooving Experimental Setup

The grooving experimental setup consisted of a Sandvik CoroCut parting blade model N123H55-25A2 mounted to a Shars SLTBN-19-6 blade holder, which was then mounted to the turret of a Boehringer turning center using a 1-inch tool holder (Figure 3.6). The parting blade was 31.9 mm in height, 3.6 mm in width and 150 mm long. For the parting blade an overhang of 50 mm was chosen as this corresponds to an overhang to width ratio of close to 14, which is already higher than the recommended ratio of less than 7. The FRF signal was obtained by means of tap tests, similar to what was explained in the previous section, but with the hammer strike occurring in the Y direction and the accelerometer mounted to measure acceleration in the X direction (Figure 3.6). The reason for this different orientation in the procedure will be explained in the next section. The acceleration in the X direction was measured by a unidirectional wax mounted accelerometer placed at the free end of the blade (Figure 3.6). This accelerometer was a PCB shear type accelerometer model 352C22 with a peak measurement range of ± 500 g, a resonant frequency ≥ 50 kHz and a frequency measurement range of 1 Hz to 10 kHz (± 5%). The hammer and the hammer tip were the same as explained in section 3.3.2, and the measurement range for this setup was also from 100 Hz to 5000 Hz. For every tap test measurement, the tightening torque on the 2 top bolts on the tool holder and the

3 top bolts on the blade holder were controlled using a mechanical torque wrench and kept constant at 11 Nm.

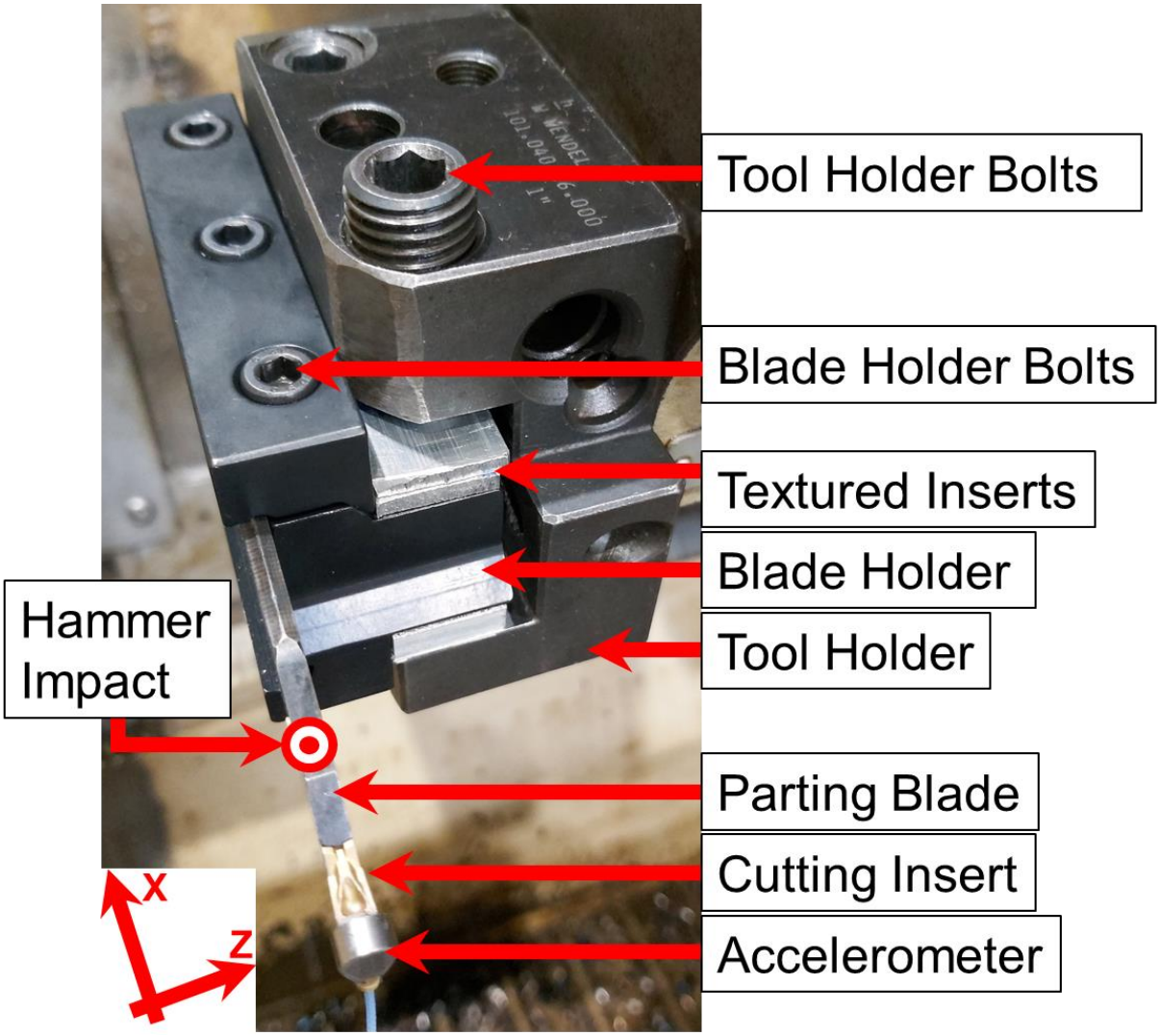

Figure 3.6 Grooving experimental setup.

From the measured FRF the damping ratio was extracted using the half power method as explained previously. With the damping ratio obtained the next step was to calculate the stability limit diagram, as described in the next section.

3.5.2 Stability Limit Diagram

The stability limit diagram for grooving/parting operations has some differences when compared with the stability limit diagram for boring operations. According to Saffury [4], for grooving tools the static flexibility in the cross FRF direction is more dominant than the direct FRF, meaning the signal to be captured for determining the stability limit should be a hammer hit in the Y direction and the displacement measured in the X direction (Figure 3.7).

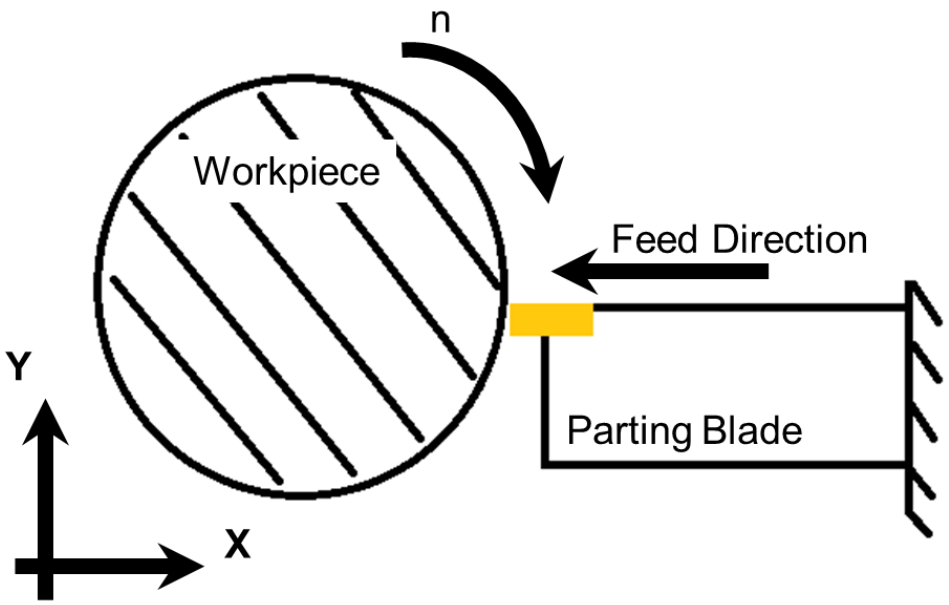

Figure 3.7 Cross section view of a parting blade operation.

Equation 3.7 used for calculating the stability limit diagram [7] [4] takes into account an oriented FRF $R_e[G_o]$ along with the specific cutting force in the tangential direction K_{ct} to calculate the limiting width of cut w_{cr} as:

$$w_{cr} = \frac{-1}{2K_{ct}R_e[G_o]} \tag{3.7}$$

where the oriented FRF $R_e[G_o]$ is calculated from Equation 3.8, G_o being the oriented FRF, $G_{xx}$the direct FRF, $G_{xy}$the cross FRF, K_{cf} the specific cutting force in the feed direction and K_{ct} the specific cutting force in the tangential direction.

$$G_o = G_{xx}\left(\frac{K_{cf}}{K_{ct}}\right) - G_{xy} \tag{3.8}$$

On account of the approximation $\frac{K_{cf}}{K_{ct}} \sim 0.3$ [22] and the static stiffness of a cantilever beam being much larger in the X direction than in the Y direction (Figure 3.7), Equation 3.7 can be approximated to Equation 3.9, where the cross FRF is used, along with only the positive values of the real part of the cross FRF $R_e[G_{xy}]$

$$w_{cr} = \frac{+1}{2K_{ct}R_e[G_{xy}]} \tag{3.9}$$

The calculated stability limit will be validated experimentally in Chapter 4.

3.6 Grooving Experiment

For grooving experiments, a Sandvik CoroCut parting blade model N123H55-25A2 was mounted to a Shars SLTBN-19-6 blade holder, the set was then mounted to the turret of a Boehringer turning center using a 1-inch tool holder (Figure 3.8). The parting blade was 31.9 mm in height and 3.6 mm in width, and was 150 mm long. The workpiece was an AISI1020 cylinder with a diameter of 63.5 mm. For all grooving experiments an overhang of 50 mm was chosen. The tightening torque on the 2 top bolts on the tool holder and the 3 top bolts on the blade holder were controlled using a mechanical torque wrench and kept constant at 11 Nm for all experiments. The machining parameters as well as other configurations and the reason behind those choices, will be presented in Chapter 4 along with the results obtained for the grooving experiments.

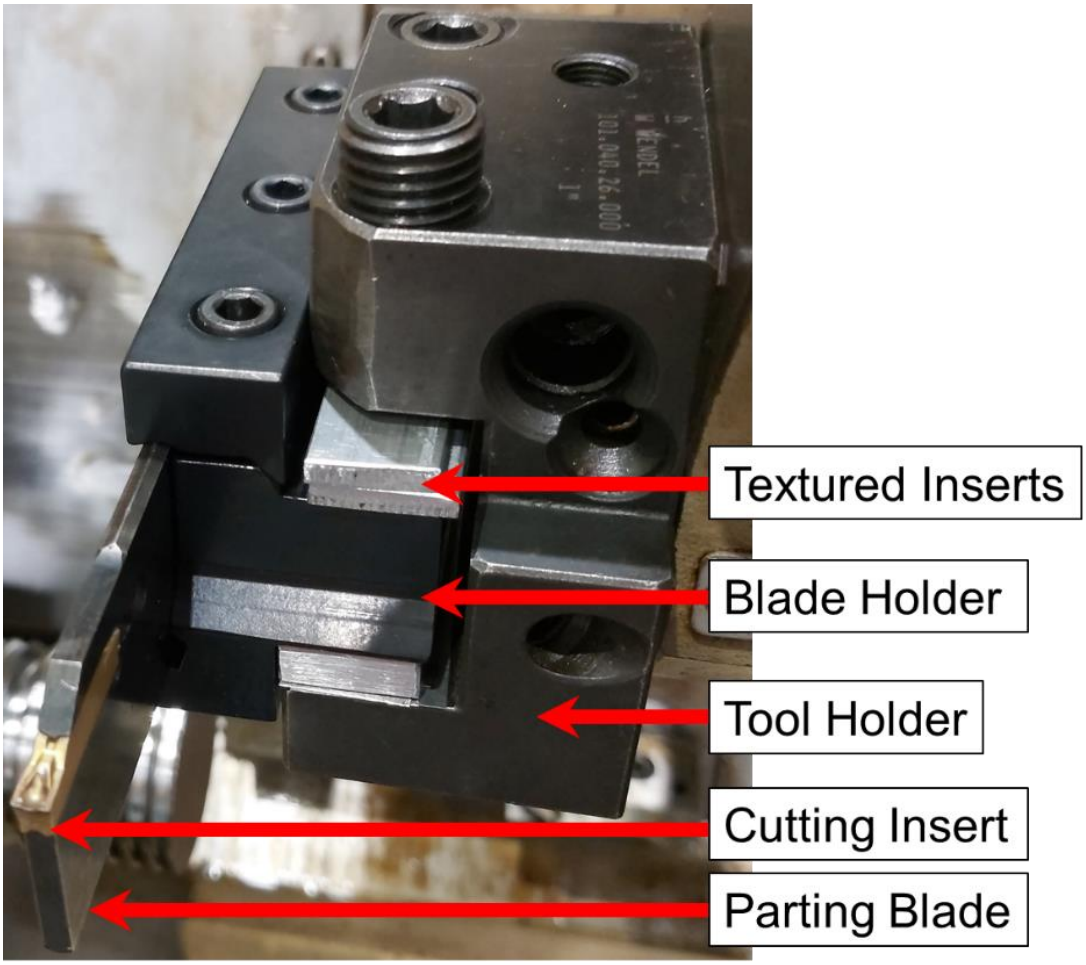

Figure 3.8 Grooving experimental setup with textured damping inserts.

Chapter 4

4 Results and Discussion

This chapter contains results obtained in this research, followed by a discussion on the findings. In the first phase of experiments, characteristics of frictional damping in the context of EDM textures were investigated. These include the effect of the position of the textured insert in the vibrating system, repeatability of damping in terms of repeated loading/unloading of the insert and tightening torque, an understanding of the damping capacity of the textured inserts with respect to their surface topographic characteristics, the effect of the textured area and the nominal pressure distribution in the contact area, and the effect of electrical discharge machining (EDM) parameters namely the discharge duration and the discharge current. In the second phase, the knowledge above was applied to enhance the dynamic stability of a grooving tool that is inherently prone to chatter, which was demonstrated through machining experiments.

4.1 Phase 1 Experiments

In the phase I experiments, a simple cantilever beam setup was used to understand the damping characteristics of EDM textured inserts, as described in Chapter 3.

4.1.1 Effect of insert and insert location

The first experiments investigated the effect of accommodating inserts in the vibrating system relative to a cold rolled steel beam with no inserts. These inserts were made either of untextured extruded aluminum or EDM-textured aluminum. Experiments also investigated the role of the insert location in the beam structure: inserts were placed either at the top or bottom of the beam (as shown in Figure 4.1), and this was evaluated against having inserts in both locations. For this experiment the EDM-textured inserts were made using a discharge time of 365 μs and a discharge current of 39 A, which was an arbitrary choice of parameters, later on this will be optimized.

The damping capacity of the inserts was assessed in terms of the damping ratio that was extracted from the frequency response functions obtained through hammer impact tests. Each measurement corresponds to the average of 5 tap tests. Figure 4.2 shows the damping ratios for the various configurations.

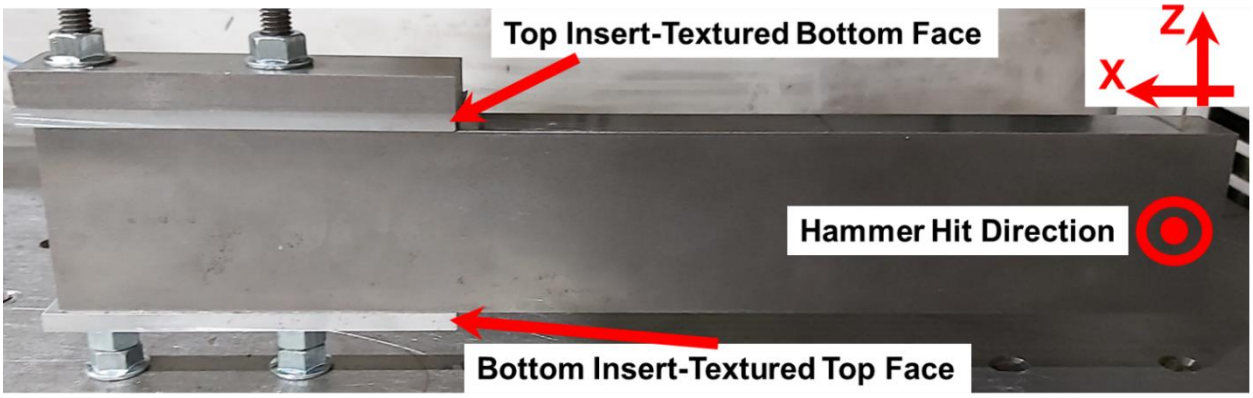

Figure 4.1 Insert placement in the vibrating beam.

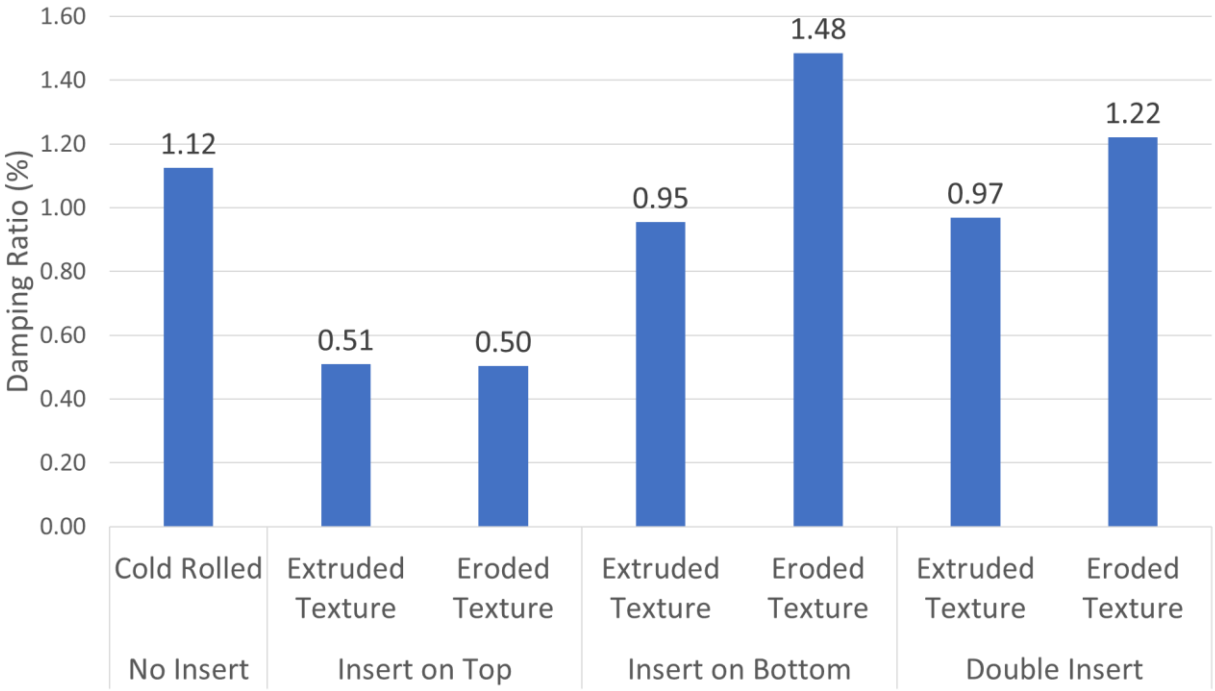

Figure 4.2 The influence of insert and insert position on the damping ratio for a direct FRF.

From Figure 4.2 it can be seen that having a textured insert on top of the beam caused no improvement in damping when compared with the situation with no inserts. This shows that having two inserts is not beneficia and led to a decrease in damping. This decrease in performance depending on insert position was also observed in the work done by Mauri *et al* [3]. Having the insert on the bottom showed an approximate 55% increase in damping, when compared with the non-textured insert in the same position. Having an insert on the bottom showed an improvement of 32% when comparing with having no inserts. Because only the insert on the bottom position was able to enhance damping there was no sense in texturing both sides of the insert, as the underside of the bottom insert would never come into contact with another surface. In order to understand the influence of textured insert position on damping, a finite element analysis was conducted using Inventor Nastran software using the beam configuration shown in Figure 4.3.

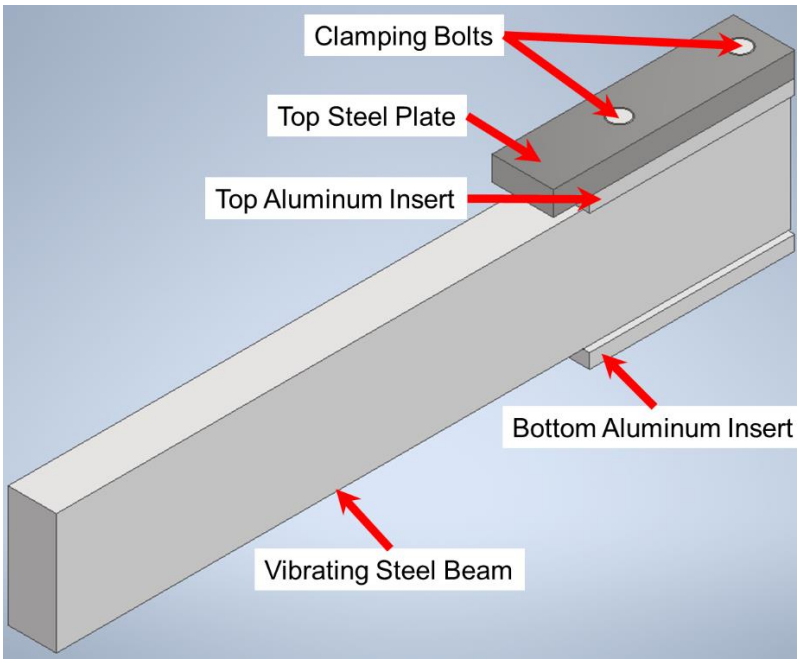

Figure 4.3 3D CAD Model in Inventor.

In the FEA model the contact between the aluminum inserts and the steel beam was configured to allow for slipping between the bodies but to avoid separation and penetration between them. For these contacts a coefficient of friction of 0.61 was used, as it was found to be the standard value for aluminum and mild steel [23]. The bottom of both bolts and the edge of the bolt holes on the underside of the bottom insert were constrained (Figure 4.4a). This simulated how the hexagonal nuts held the experimental beam in place. The clamping force exerted by the top nuts was simulated as a force pushing down against the edge of the bolt holes on the upper face of the top insert, as illustrated by the black arrows in Figure 4.4b. The bolt load applied by the top nuts was simulated by applying a pulling force on the top face of the bolts, as illustrated in Figure 4.4b by the orange arrows. The bolt load was calculated using equation 4.1, where *F* is the bolt loading force, *T* is the torque applied on the top nuts, *K* is a constant depend on thread conditions and *d* is the nominal bolt diameter. To calculate the bolt load, a *K* constant of 0.2 was used [24], along with a *d* of 0.008 m and a *T* of 11.3Nm, as it was the torque applied on the real setup. Using those values on equation 4.1 gave an axial load of 7063 N.

$$F = \frac{T}{K \cdot d} \tag{4.1}$$

A model transient response analysis was conducted on the FEA model to mimic a tap test procedure. Various model transient response analyses were conducted while varying the mesh size on the model, in order to determine the correct mesh size. The

FEA model was validated by comparing the natural frequencies of the first three modes with those from the experimental setup (Figure 4.5). Table 4.1 presents a comparison of these frequencies which shows good agreement.

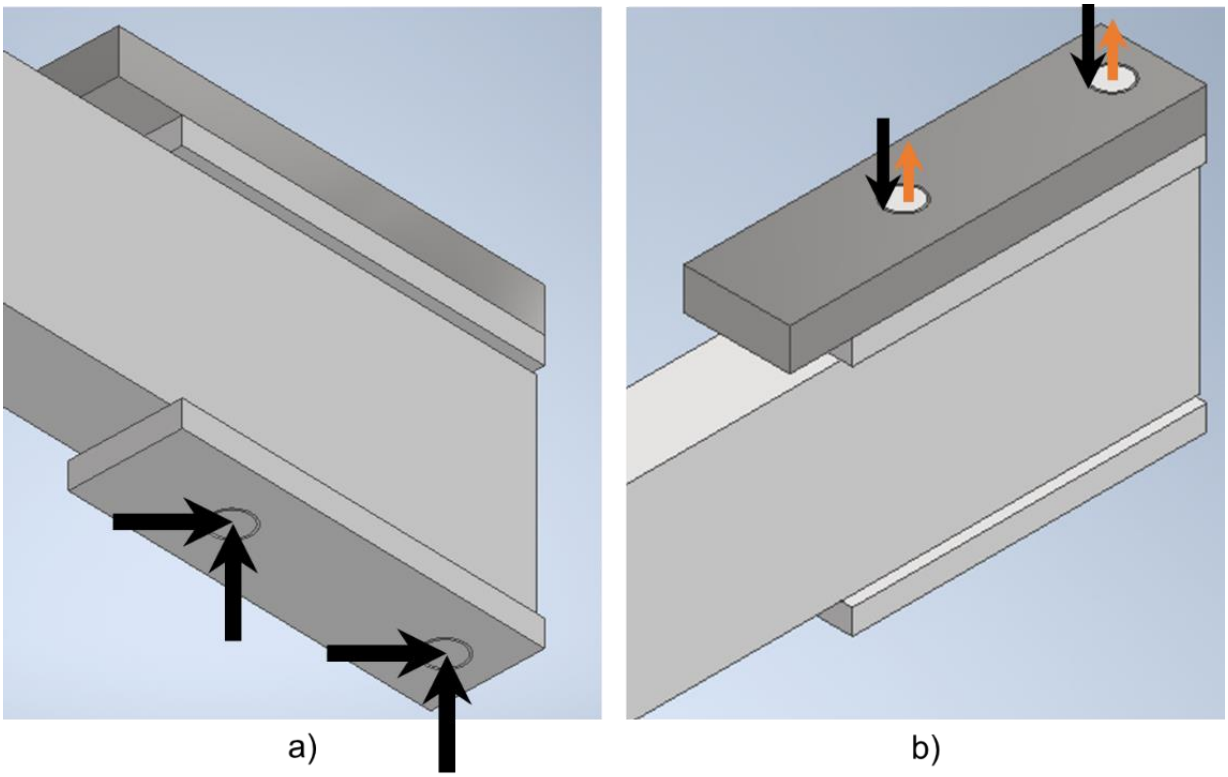

Figure 4.4 a) Applied Constraints. b) Bolt loads

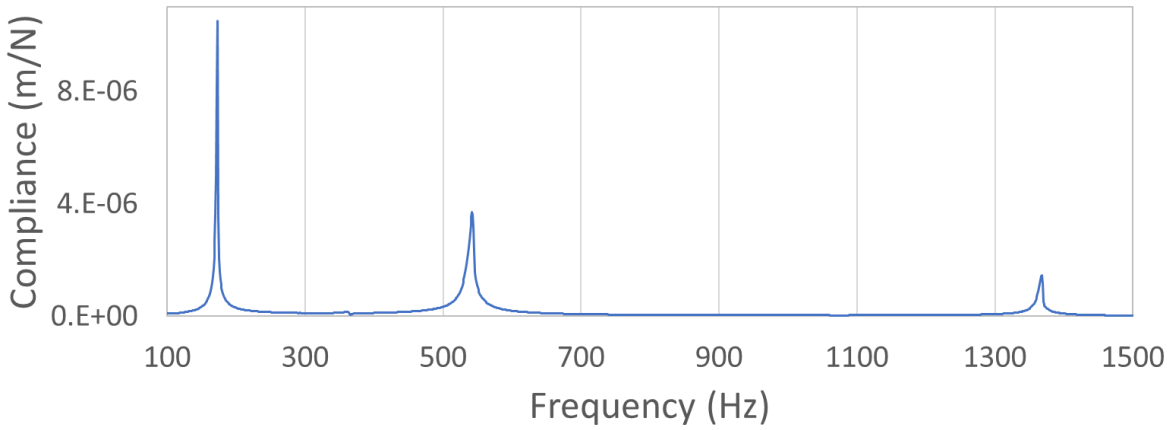

Figure 4.5 FRF from experimental setup.

	Experimental	FEA Model
Mode	Frequency (Hz)	Frequency (Hz)
1	175	188
2	540	590
3	1370	1391

Table 4-1 Comparison of natural frequency from FEA model against experimental values.

Subsequently, an analysis was conducted to determine the relative motion between the steel beam and both the top and bottom inserts. This was done by selecting one point from the top face of the beam and one point from the bottom face of the top

insert, as shown by the green arrows in Figure 4.6. This was repeated for the bottom side of the beam by selecting one point from the bottom face of the beam and one point from the top face of the bottom insert, illustrated in Figure 4.6 by the red arrows. Finally, the displacement of those four points in the X direction (parallel to the application of the impact load) was plotted as a function of time (Figure 4.7).

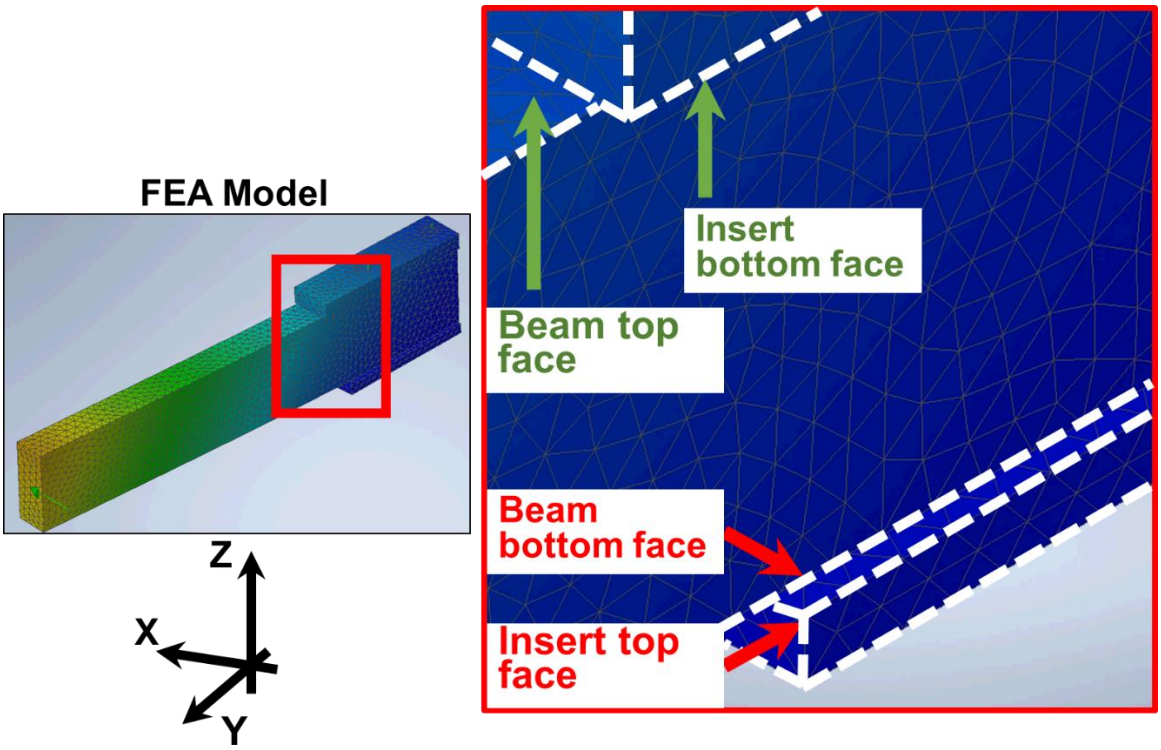

Figure 4.6 Points selected for the point displacement study.

Figure 4.7 shows that there is a larger relative displacement between the bottom set of points than between the top set of points. This result allows for the conclusion that the larger relative displacement and hence more microslip between the two bottom points is what makes the bottom insert outperform the top insert in terms of damping enhancement. This conclusion means that for a real-world application of this technology a similar dynamic study would have to be performed in order to determine the correct placement of the textured insert.

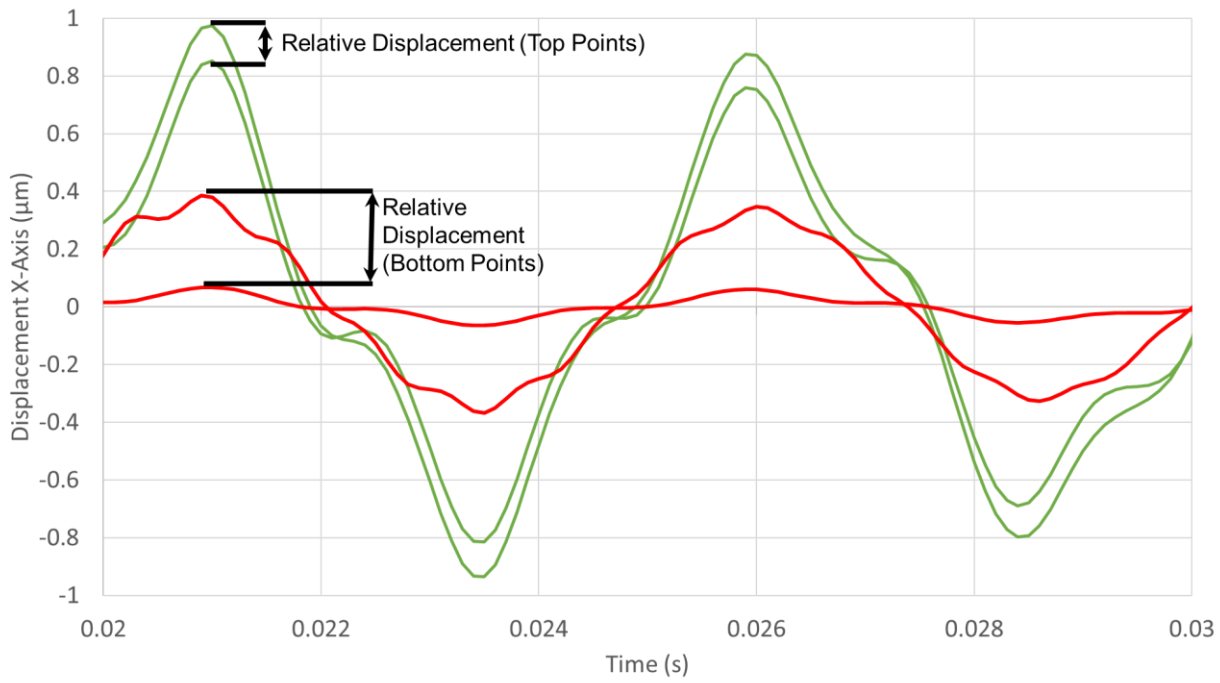

Figure 4.7 Relative displacement between point pairs.

A different tap test orientation was also tested as to investigate how the texture would perform. This new tap test orientation consisted of hitting the steel beam in the negative Z direction (Figure 4.1). The accelerometer was also moved. Instead of having

the accelerometer mounted to the opposite side of the striking face, capturing oscillations in the same direction as the hammer hit, this time the accelerometer was mounted in the free end perpendicularly to the striking face as to capture motion in the X direction (Figure 4.1). Results from this tap test (Figure 4.8) shown the bottom insert outperforming the top one as before. The explanation for this is the same as the one previously discussed. Damping ratios obtained from this new tap test are lower than the ones seen in the previous tests. This is because the bending stiffness of the beam in the Z direction is larger than in the X direction, thus the same impact force causes less deformation on the beam, consequently leading to a smaller amplitude of vibration. This smaller amplitude leads to less relative displacement and hence less microslip between the insert and the beam.

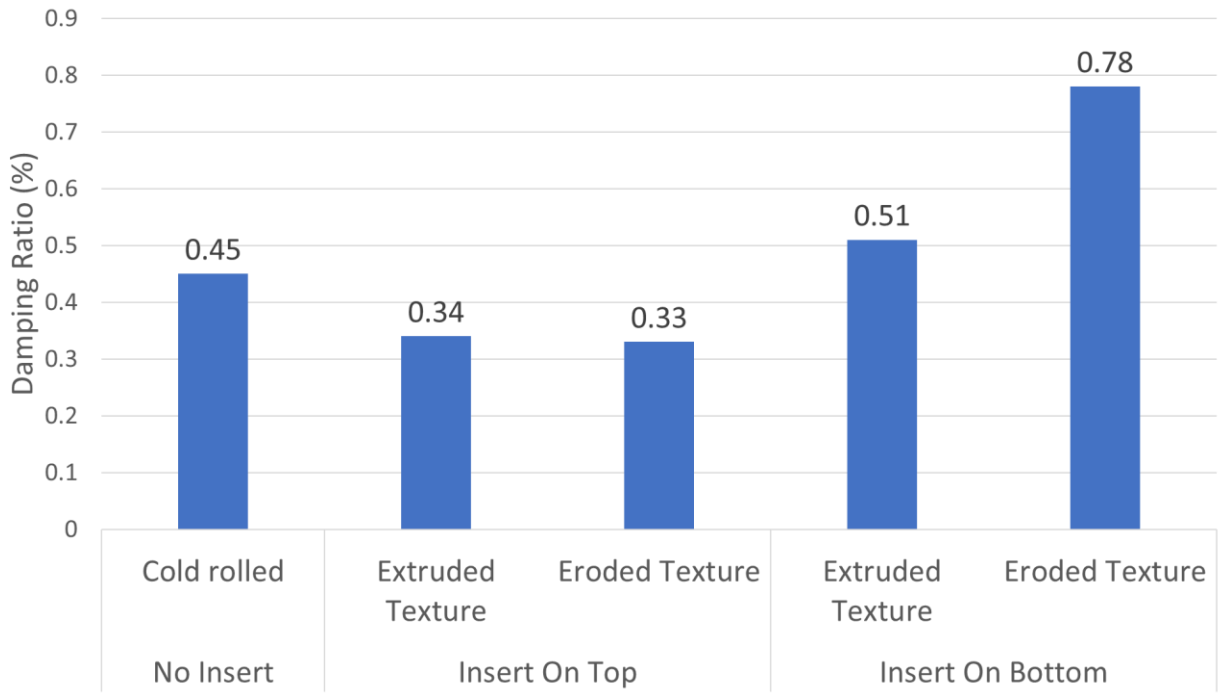

Figure 4.8 Influence of insert and insert position on damping for a cross FRF.

4.1.2 Process Repeatability and Effect of Tightening Torque

The next investigation was done to determine the repeatability of the results when the setup was disassembled and reassembled, as well as to determine the influence of changing the tightening torque on the clamping bolts. For this experiment the EDM-textured insert was made using a discharge time of 65 μs and a discharge current of 72 A. This texture was chosen because it had shown good performance on previous tests.

Five cycles of assembling and disassembling were conducted on the setup using the same textured insert. On the third assembly cycle the tightening torque on the clamping bolts was increase by 10 kN, to determine how the increased contact pressure would affect damping as well as to determine if the higher contact pressure would damage the texture and affect its performance.

On the first part of this experiment the textured insert was mounted at the bottom of the assembly and the clamping bolts were tightened to 11 Nm. Subsequently eight tap tests were conducted on the structure obtain the damping ratio for that texture. The entire setup was then disassembled, and the process repeated for the second cycle. In the third cycle everything was repeated following the same procedure as previously explained, with the only difference being the tightening torque on the clamping bolts, which was increased from the previous 11 Nm to 21 Nm. The fourth and fifth experiment were conducted exactly as the first and second cycle, with the tightening torque lowered back

to 11 Nm. The results obtained for each of the tap tests in every cycle is presented in Figure 4.9

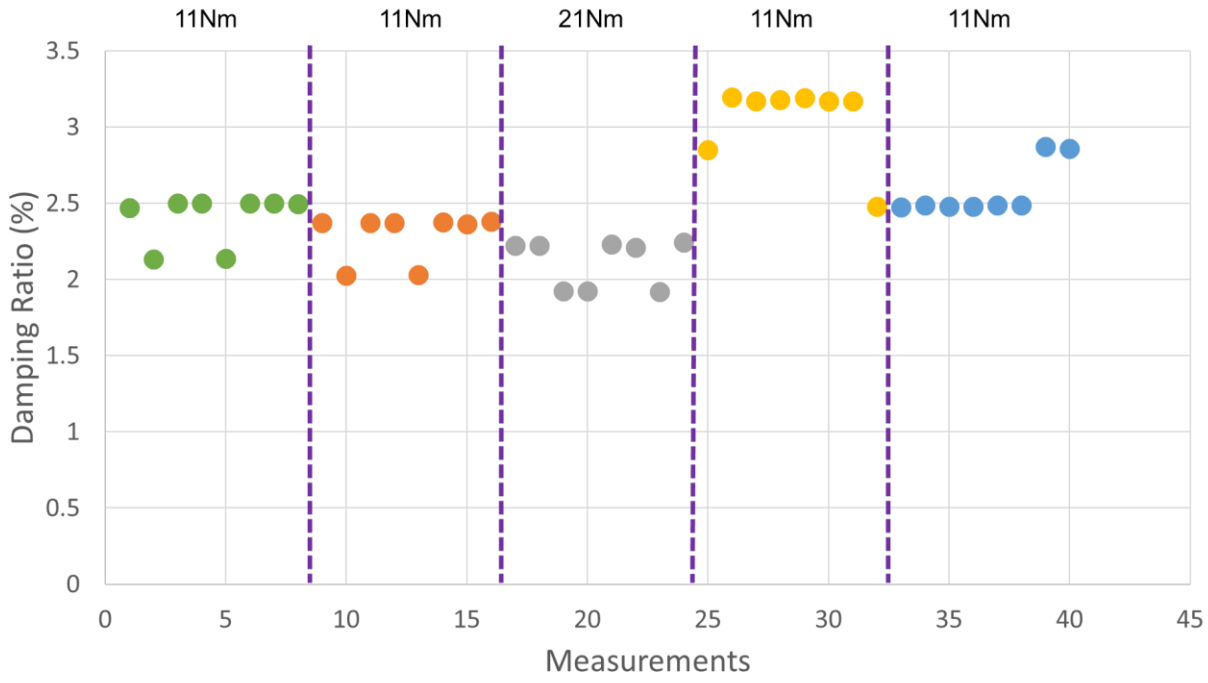

Figure 4.9 Repeatability of damping and the influence of bolt torque.

From Figure 4.9 it is possible to conclude that the process is repeatable across several cycles of assembly and disassembly, which is very significant from an application perspective. Increasing the tightening torque reduced the damping as expected due to the tendency for reduced microslip, as has also been reported in previous studies [3][16]. The higher clamping pressure did not affect the texture performance negatively, it did in fact enhance it somewhat on the subsequent loading cycles. Further work is required to understand this behavior. Figure 4.9 show higher damping values than the ones on Figure 4.2 because the insert texture used for this experiment outperforms the one used on that experiment; this is further investigated in the subsequent section.

4.1.3 Effect of EDM Parameters on Damping

In order to determine the influence of eroding parameters on damping, discharge time and discharge current were varied systematically over a wide range to obtain surfaces with varied topographic characteristics. For this part of the study three current levels were investigated: 21 A, 39 A and 72 A, along with eight different discharge durations: 12, 32, 65, 116, 154, 178, 205 and 237 µs. Figure 4.10 shows the damping ratio obtained for each of the textures.

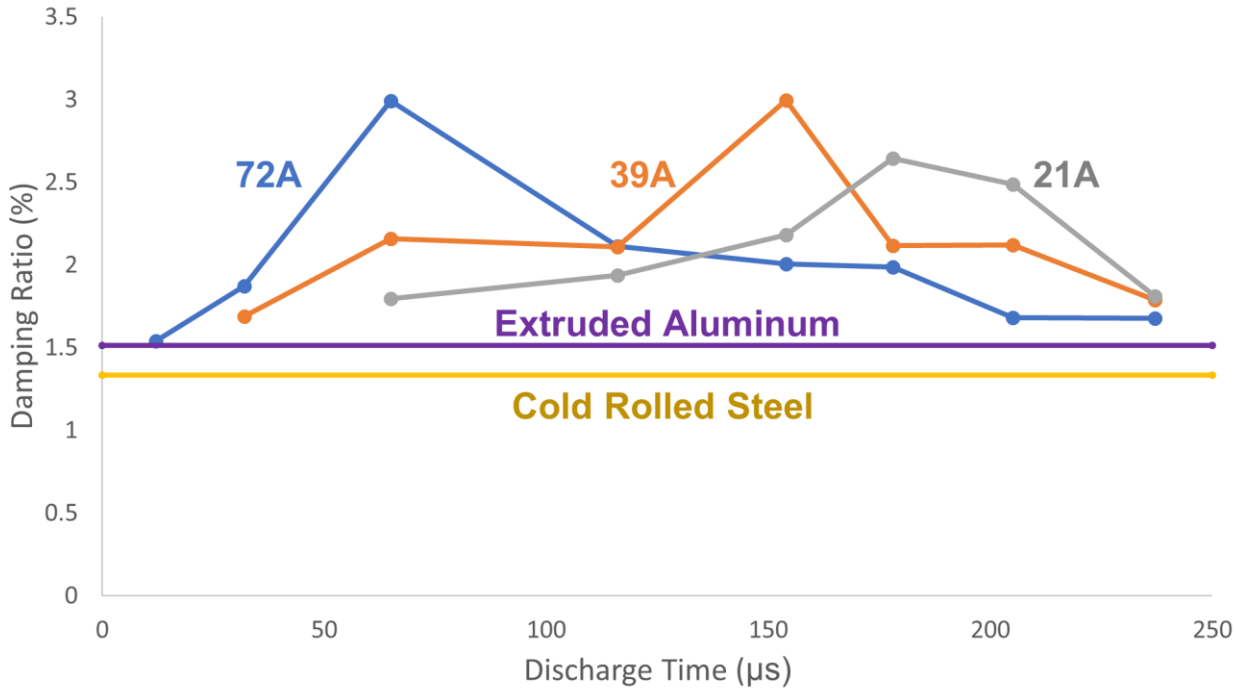

Figure 4.10 Effect of eroding parameters on damping ratio.

Figure 4.10 shows the best performance was obtained at a current of 72 A when using a discharge duration of 65 µs. When decreasing the current to 39 A, a similar performance was achieved at a higher discharge duration. From Figure 4.10 it can be seen that an optimum combination of current and duration is required in order to achieve

the highest damping ratio. With decreasing current, the best performance shifts to higher discharge durations.

Figure 4.10 highlights the fact that the innovative application of EDM texture in enhancing damping is interesting also from the viewpoint of EDM, considering that its relatively low material removal rate is of little consequence in such texturing applications that involve an insignificant removal volume. In this case, a textured insert could be produced in a matter of several seconds. Surface integrity issues that could arise in EDM under high discharge energy conditions are also not of concern in this application since the loading in this instance is not tensile. EDM process parameters viz., the discharge current and duration, may further be readily manipulated to tailor the crater geometry at a fine scale towards maximizing the damping capacity of the surface.

4.1.4 Investigation of Surface Characteristics

The topographic characteristics of surfaces generated in the experiments that examined the effect of discharge current and discharge duration were analyzed using a confocal microscope to understand damping at a fundamental level. Specifically, the average roughness parameter *Sa*, the skewness *Sk* and kurtosis *Rk* were considered.

Figure 4.11 shows a plot of damping ratio as a function of surface roughness which indicates the lack of any systematic correlation. It is clear that surfaces with essentially the same *Sa* value could correspond to damping ratios that are different by a factor of 2. This also highlights the drawback of the works of Beards et al [21] who reported damping

in terms of just roughness values, while only considering textures that were generated from changing the discharge current.

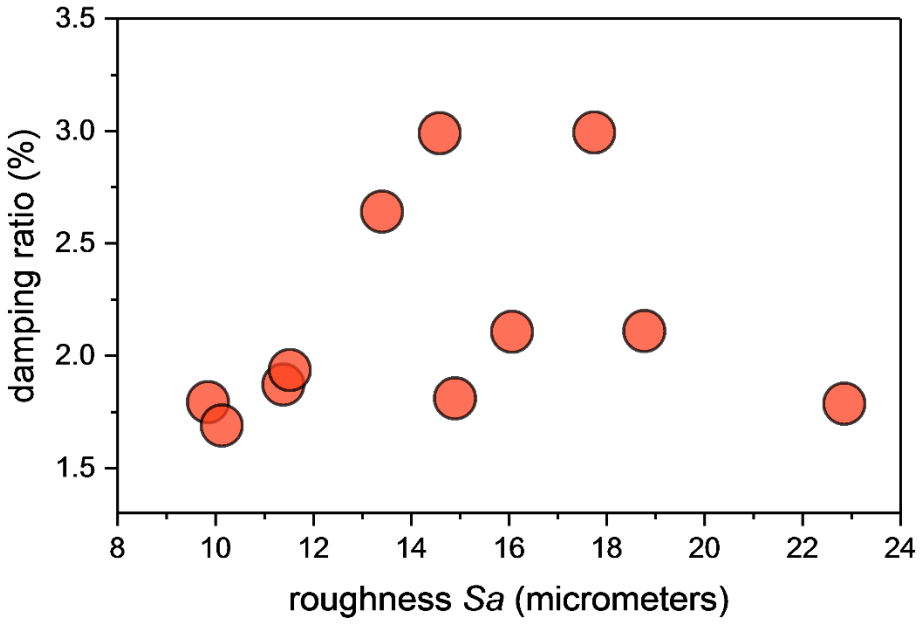

Figure 4.11 Damping ratio as a function of average surface roughness.

Having found no systematic correlation of damping with the average roughness, the next step was to evaluate the effect of surface skewness and kurtosis on damping. Figure 4.12 presents these results in a three-dimensional plot, which shows the damping to increase modestly with an increase in both skewness and kurtosis values. The damping ratio is but significantly maximized at high values of skewness and kurtosis, due to the significant interaction between these indices. This is quite in alignment with the work of Medina *et al.* [19] who through numerical simulations predicted the energy dissipation to increase with increasing kurtosis and increasing positive skewness (Figure 4.13). The surfaces created in EDM can be seen to have positive skewness, which is a unique and

valuable characteristic of EDM in this application. This information also provides clues for the design of surfaces to further enhance damping in terms of surface characteristic parameters.

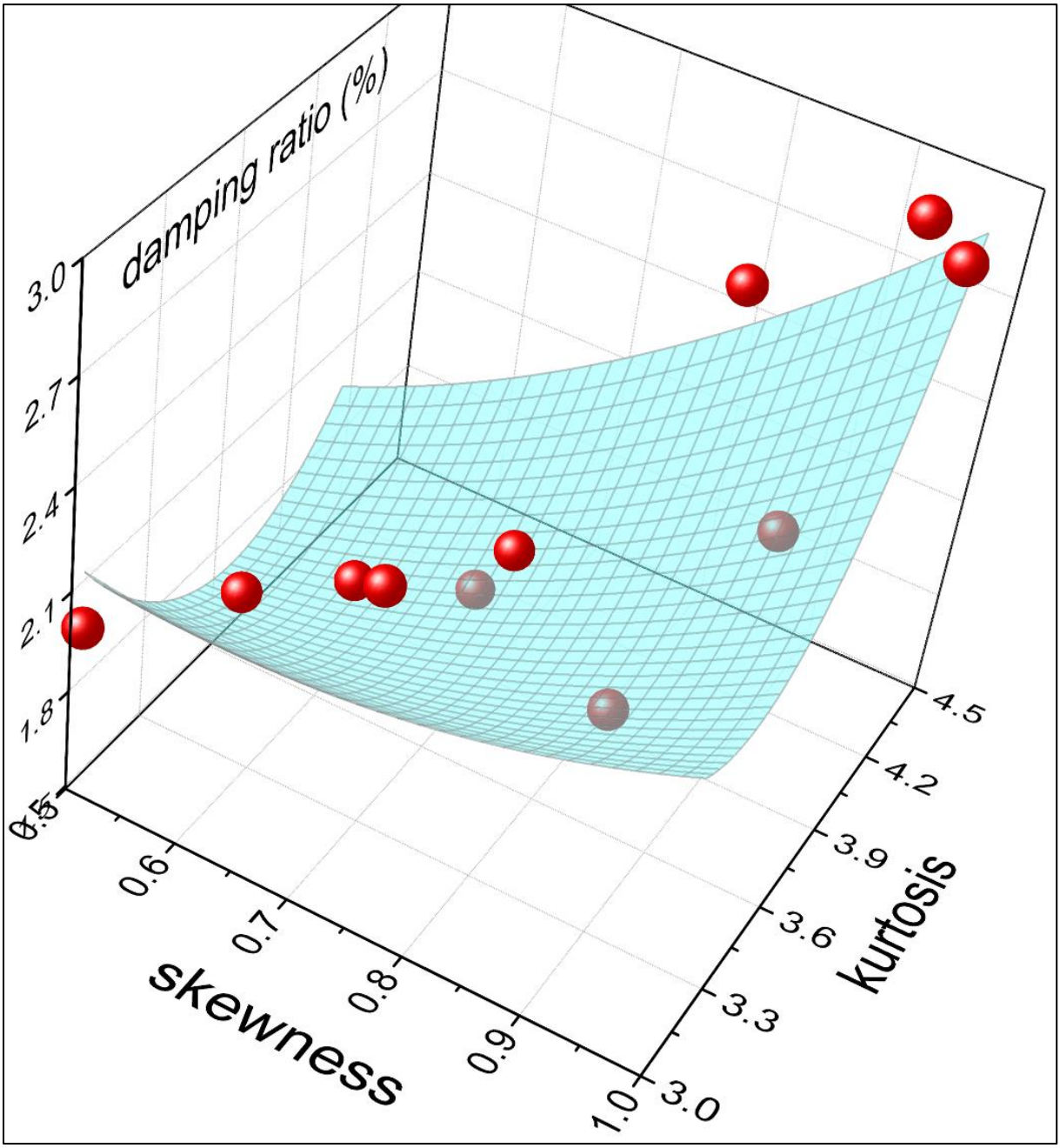

Figure 4.12 Damping ratio as a function of skewness and kurtosis.

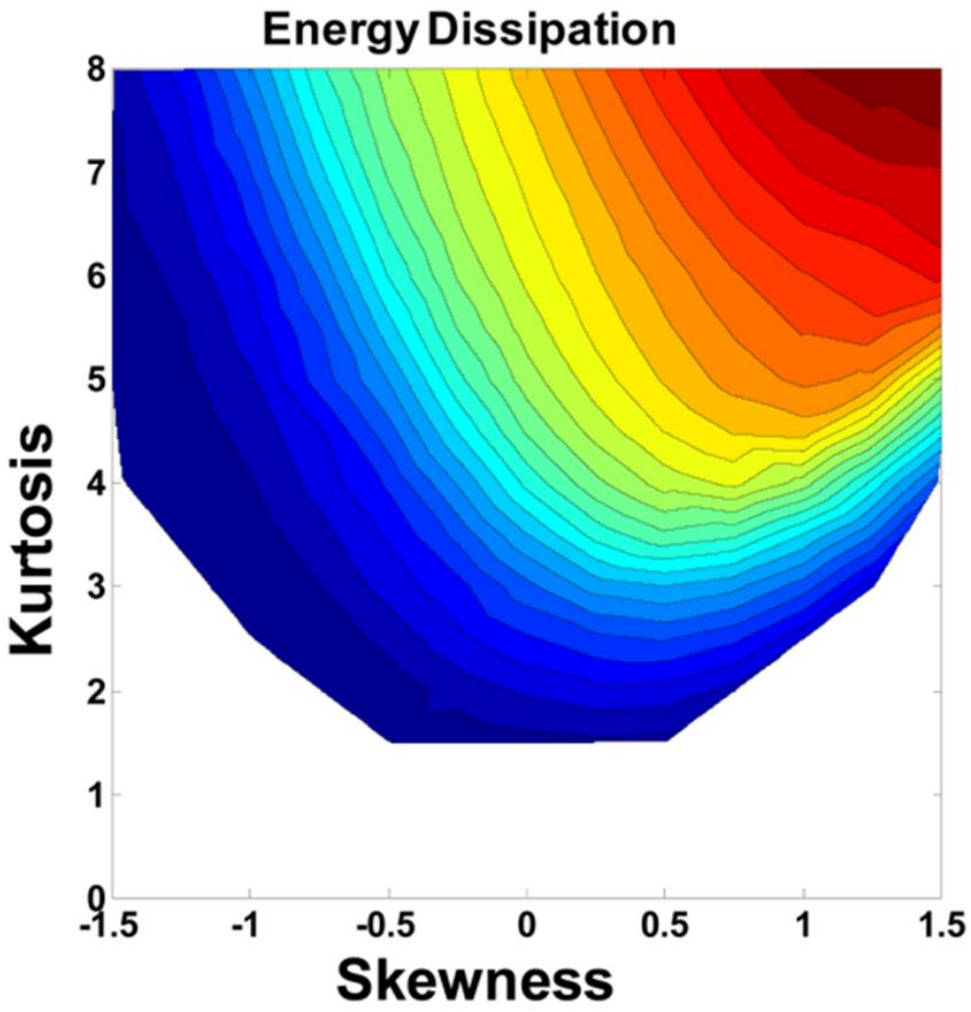

Figure 4.13 Effect of kurtosis and skewness on energy dissipation [4].

Figure 4.14 shows the three-dimensional view of the surface that corresponded to a discharge current of 72 A and a discharge duration of 65 µs. The figure shows isolated peaks among a large number of valleys as signified by the positive skewness and high kurtosis. Such peaks anchor themselves against a counterface to transfer the loads and provide the required tangential and normal stiffness, while providing damping through a micro-slip mechanism.

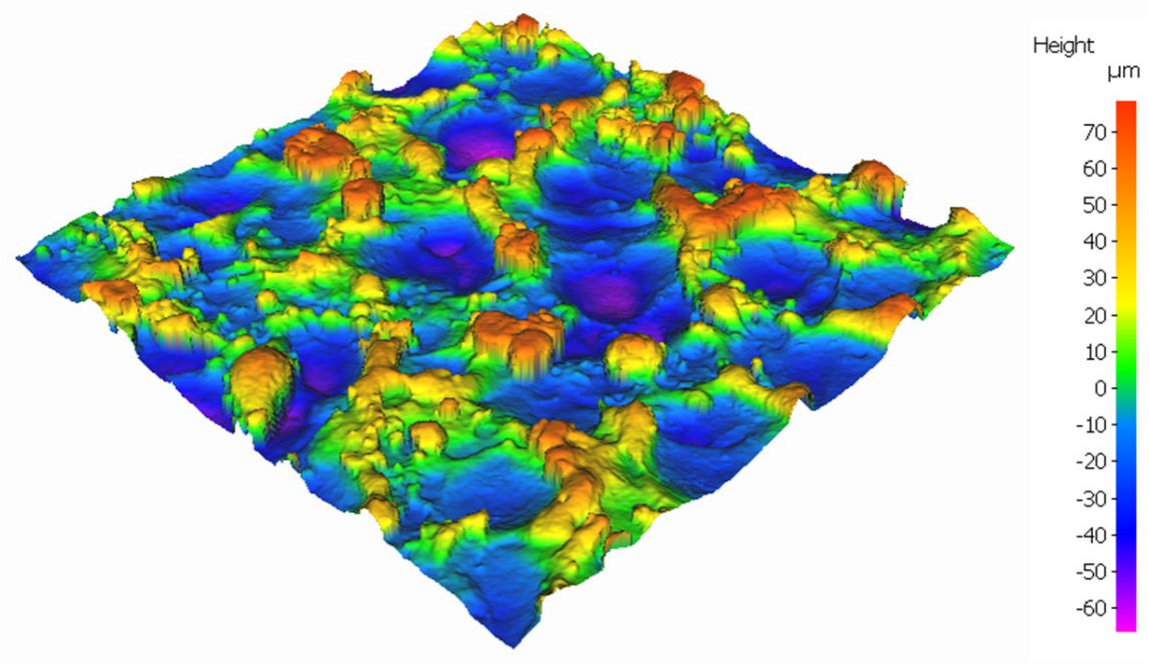

Figure 4.14 3D surface scan of the best performing surface texture.

4.1.5 Effect of Textured Area

To study the effect of textured area on damping, four inserts with identical width and lengths of 65, 73, 85 and 100 mm were cut. The inserts were then textured with a discharge current of 72 and a discharge duration of 65 µs that pertained to the highest damping. The extracted damping ratios under a constant tightening torque on the clamping bolts are presented in Figure 4.15, which shows the damping to increase with area, reaching a maximum value of 4.5% which represents an enhancement in damping ratio of over 400% of that of the baseline (Figure 4.2). Additional work is required to understand if the increase in damping is actually due to a reduction in the nominal pressure across the interface.

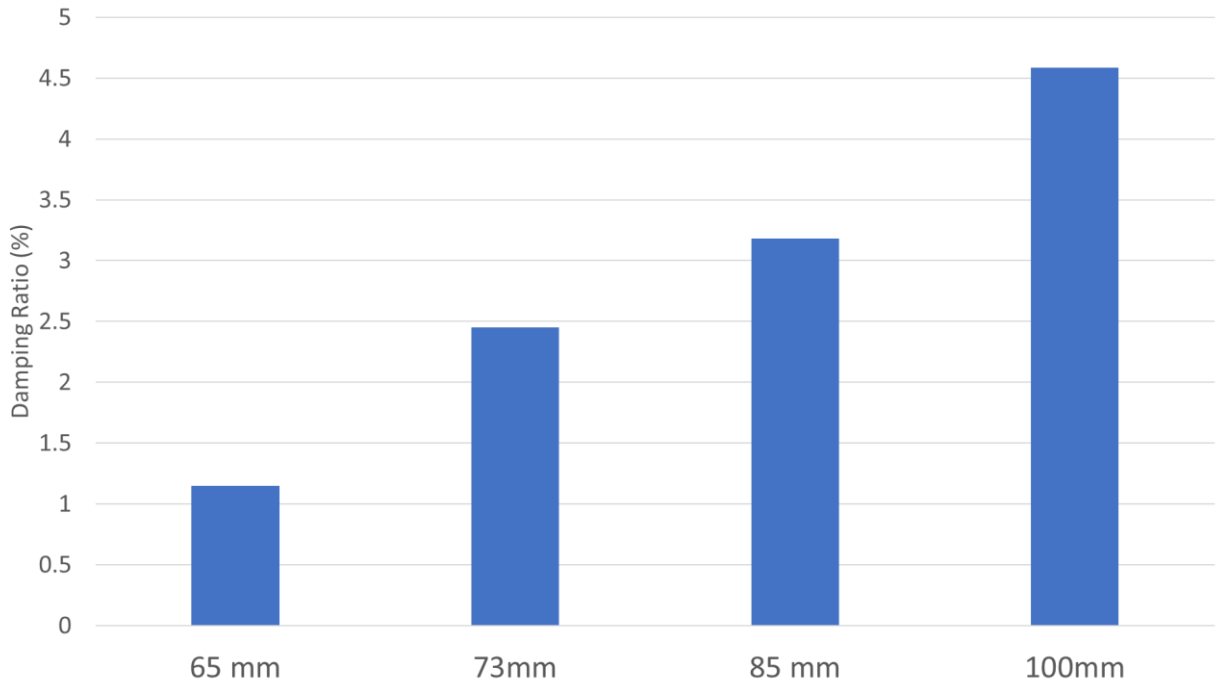

Figure 4.15 Effect of textured area on damping ratio.

4.1.6 Effect of Pressure Distribution

The last investigation carried out in this phase of the research focused on evaluating the effect of pressure distribution at the contacting interface. Following the work of Wentzel *et al.* [18], the pressure distribution was altered by drilling an array on holes on five textured inserts. To maintain comparable textured area, the size of the drilled holes and the number of drilled holes were determined in such a way as to always remove approximately 25% of the textured area on each insert. Table 4.2 shows the number of holes drilled, their diameters and the consequent area reduction for each of the tested inserts. After the inserts were eroded with the best performing texture and before drilling the holes, every insert went through five tap tests to determine their damping ratios before

the holes were made. Because the five tested inserts were eroded with the same texture, this first set of tests also shows the insert-to-insert variability.

Hole Diameter (mm)	Number of holes	Final Area	% Reduction	Textured Insert
3.96	32	1671.88	0.19	V9
5.95	14	1676.73	0.19	V6
7.93	8	1670.88	0.19	V8
9.1	6	1675.77	0.19	V5
12.7	3	1685.97	0.18	V7

Table 4-2 Number of drilled holes, their diameters and area reduction for each insert.

After drilling all the holes each insert was tap tested five more times and the new damping ratios calculated. Results obtained for the inserts with and without holes are presented in Figure 4.16, where each color corresponds to the same textured insert without holes (the set on the left side) and with holes (the set on the right side). The insert-to-insert variability can be seen on the left-hand side graph.

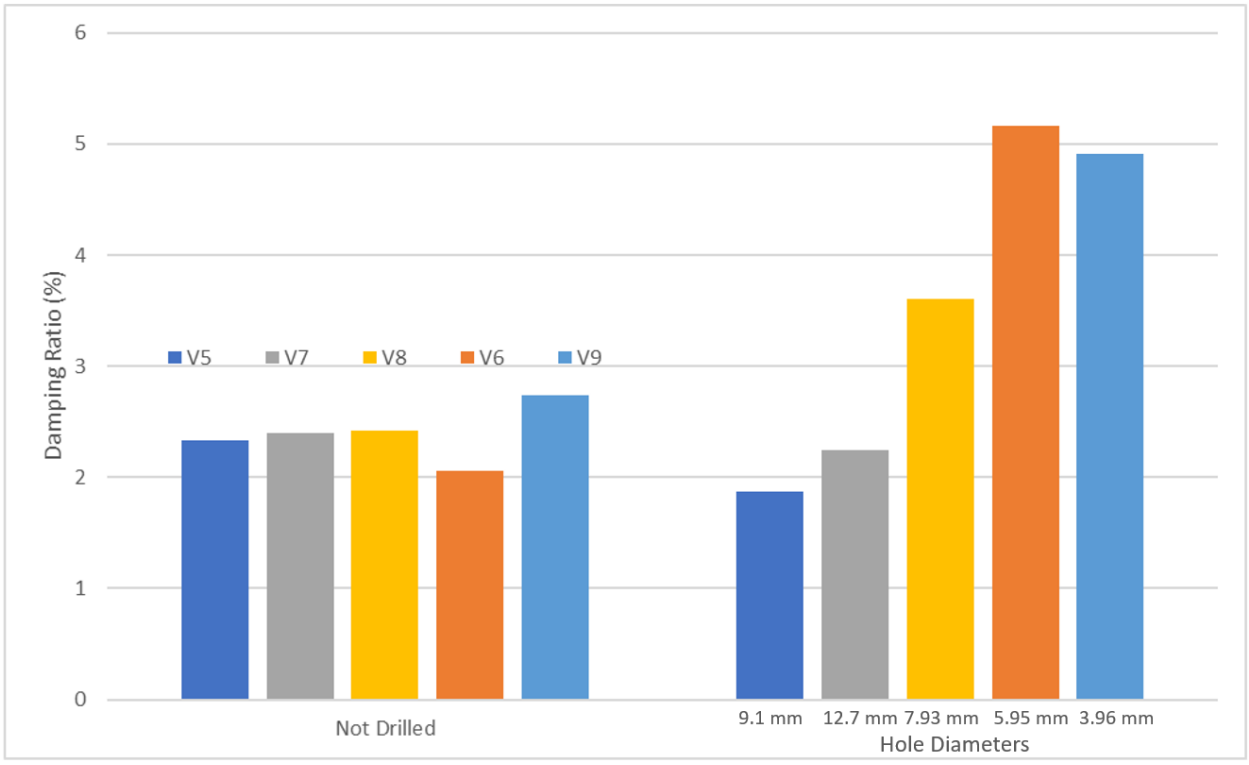

Figure 4.16 Insert-to-insert variability and effect of pressure distribution.

When comparing the situations with and without holes for the same insert it is clear that damping performance decreased with respect to the baseline for inserts V5 and V6 which corresponded to the larger diameter of drilled holes. With a reduction in the diameter of the holes, however, a significant increase in damping was obtained, to the tune of about 250%.

Stachowiak *et al.* [25] explained the effect of such holes on damping. They showed that whenever two surfaces are in contact, the normal stress (*W)* on the contact area smoothly increases from zero, at the edges of the contact area, to a maximum value at the center of the contact (Figure 4.17a). While stresses tangential to the contact area (*Q*)

will follow the opposite direction, thus growing from a minimum value in the center of the contact, to a theoretical infinite value at the edges of the contact (Figure 4.17b). Since frictional force is the product of the coefficient of friction (μ) and the normal stress, this means that at the edges of a contact the tangential stresses will surpass the frictional force thus generating microslip (Figure 4.17c). Consequently, by drilling holes on the textured area it is possible to generate more regions that behave like edges of the contact area and so have a larger area where microslip can happen. Smaller holes have better performance as more holes will fit in the same area, increasing the region where microslip can happen. This conclusion can be backed by the graph shown in Figure 4.18, where damping ratio was plotted as a function of hole diameter. The graph in Figure 4.18 show a significant increase in damping as the hole diameter decreases, illustrating how smaller holes are more beneficial towards increasing damping.

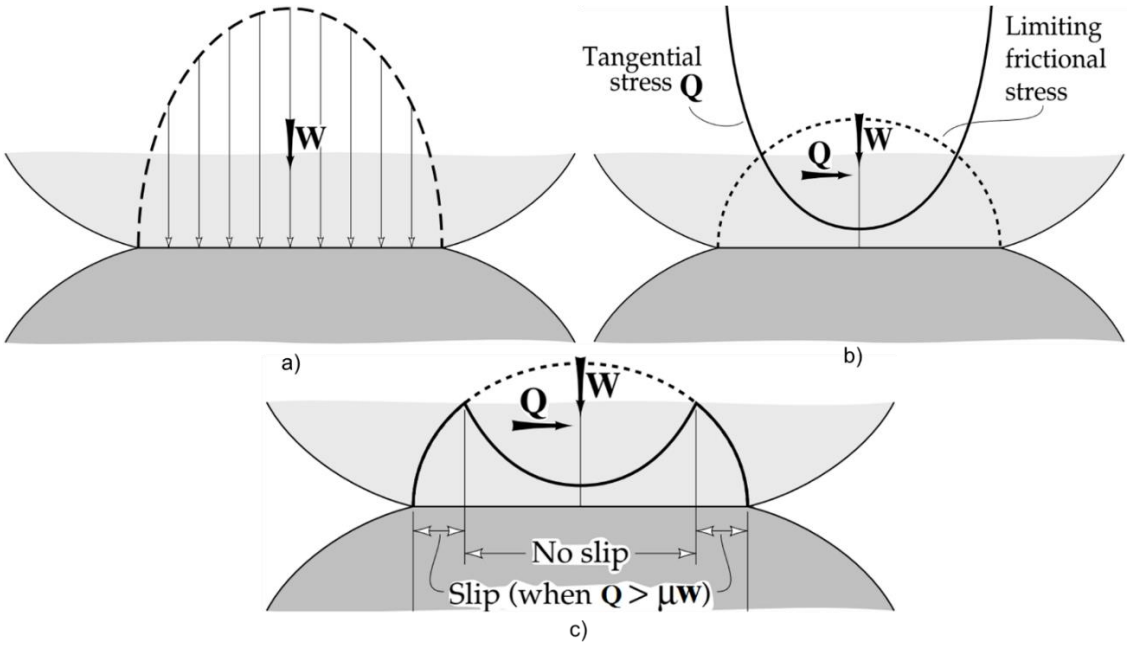

Figure 4.17 a) Normal stress distribution. b) Tangential stress and limiting frictional stress. c) Slip and No Slip regions in the contact area [25].

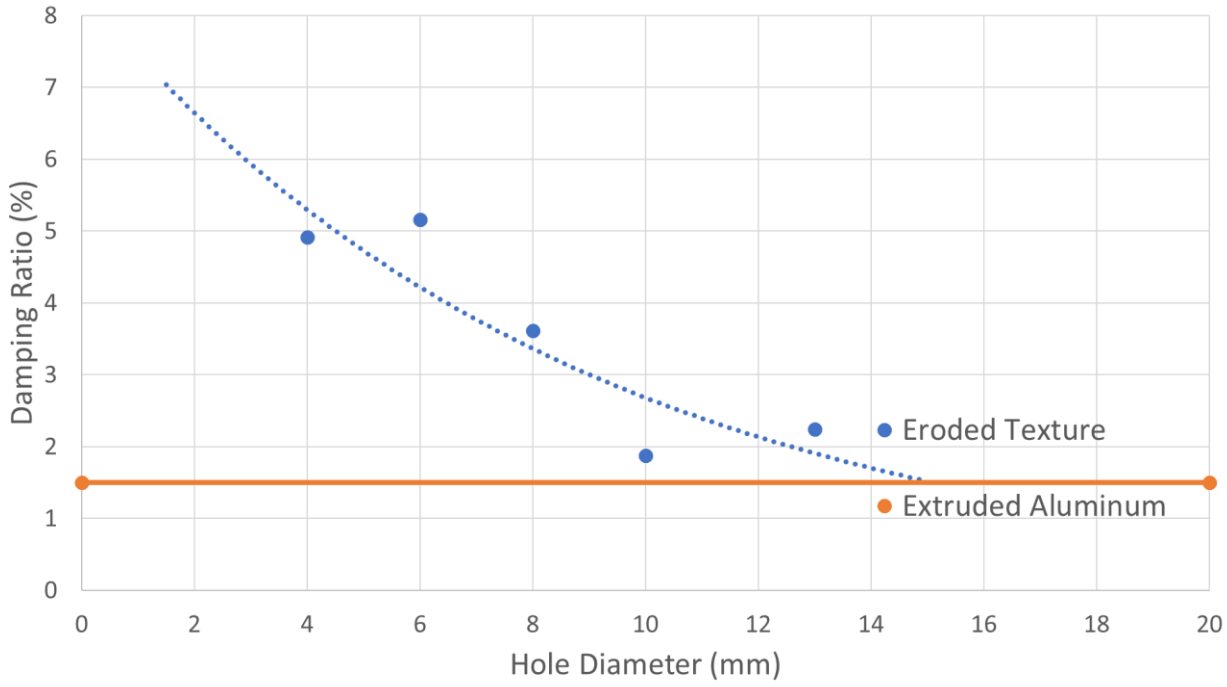

Figure 4.18 Effect of hole diameter on damping.

Having understood the effects of several parameters on damping in the Phase I experiments, the next phase, presented in the subsequent section, focused on applying the technology to a grooving tool in order to enhance its dynamic stability, given that this tool is inherently prone to chatter.

4.2Phase II: Application

In this phase of the research, three grooving experiments were conducted to prove the concept of using EDM textures to control vibration and enhance tool dynamic performance. The first experiment served as a baseline, and referred to a commercial grooving tool used in industry that is made from ground steel. The second was a control experiment, which involved stacking of two extruded aluminum damping inserts on top of

the blade holder and one extruded aluminum damping insert located beneath the blade holder (Figure 4.19). The stacking of inserts in this experiment was done as to increase the textured area, since the study presented in section 4.1.5 showed a possible direct correlation between textured area and damping ratio. The last experiment pertained to the said damping inserts textured using EDM on particular faces as shown in Figure 4.20. The surfaces were eroded using a discharge current of 72 A and a discharge duration of 65 µs, as these were the best performing parameters found by the investigation presented in section 4.1.3. Figure 4.20 also shows one of the damping inserts in which 32 4-mm holes were drilled, this was the best number of holes and hole diameter combination obtained from the investigation done in section 4.1.6.

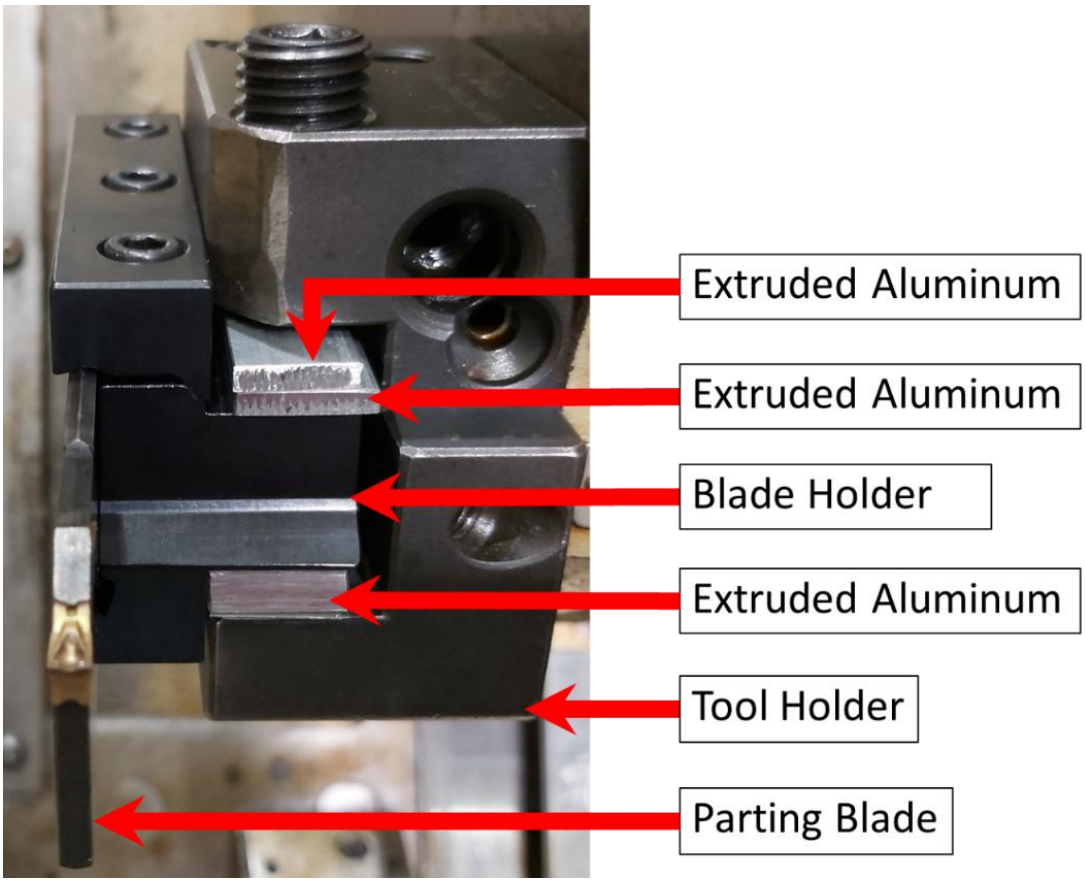

Figure 4.19 Tooling configuration of control experiment.

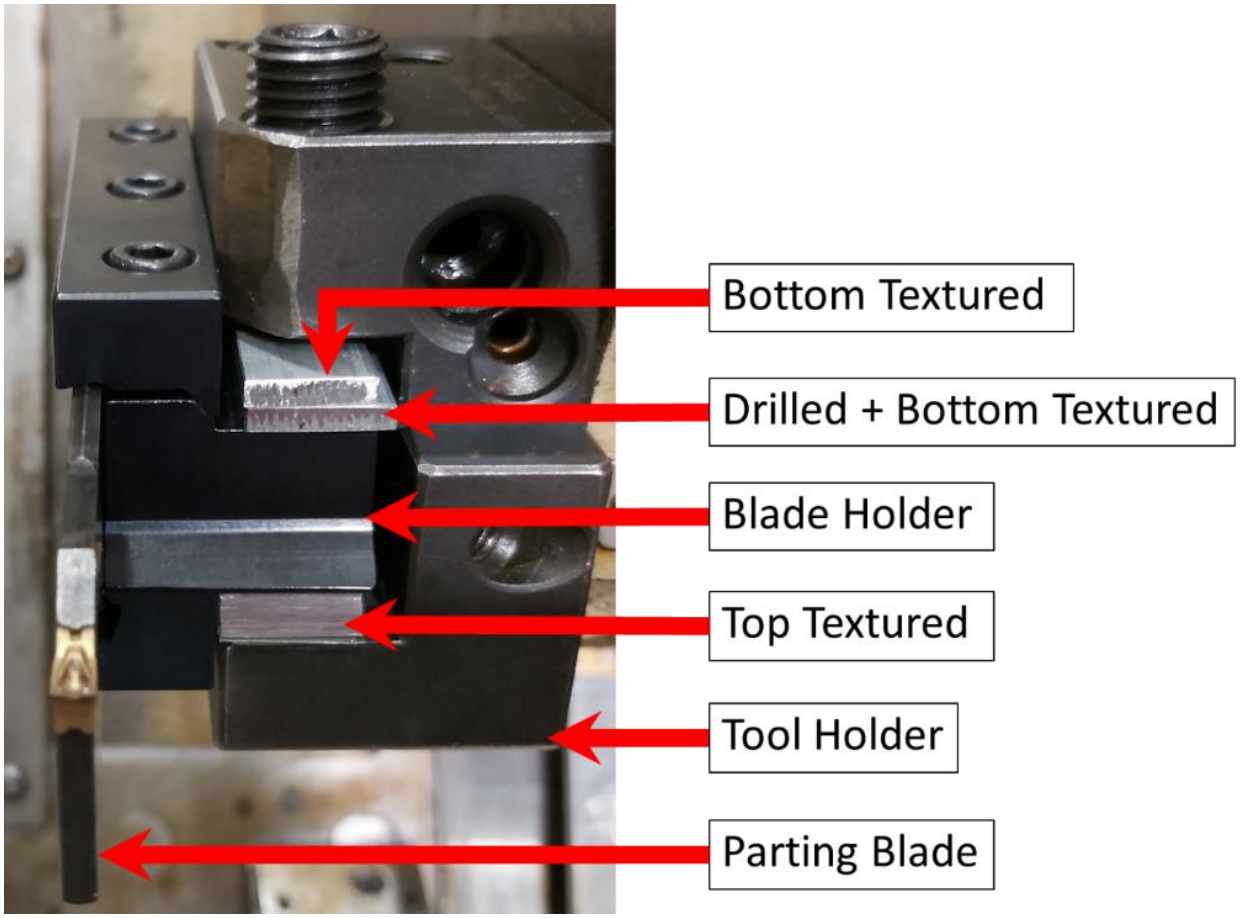

Figure 4.20 Tooling configuration for proof of concept.

Tap tests were conducted for each of the three configurations. From these tests frequency response functions were obtained (Figure 4.21), which illustrate the dynamic stability of the configurations.

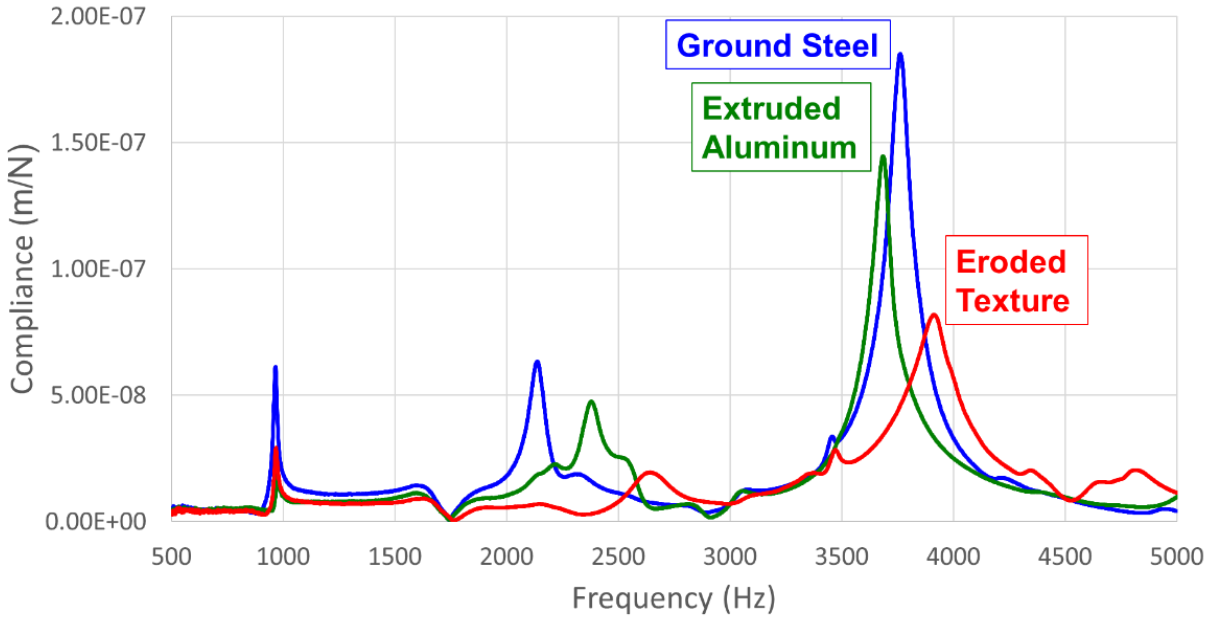

Figure 4.21 FRF corresponding to the three experimental configurations.

The peaks present in Figure 4.21 refer to modes where the system is dynamically unstable, and thus susceptible to vibration. The higher the peak, the more unstable the system is at that frequency range. Figure 4.21 indicates the grooving setup to have three critical peaks for all three configurations. The first peak is in the range from 900 Hz to 1100 Hz, the second peak in the range from 2000 Hz to 2700 Hz and the third peak in a range from 3500 Hz to 4000 Hz. Figure 4.21 clearly shows the eroded texture to have been able to enhance the dynamic performance of the system in all three modes relative to the commercial tool and the control. The third mode of vibration is the critical mode that exerts the most influence on the dynamic behavior of this tooling system.

From the information pertaining to the critical (third) mode in the FRFs, stability lobe diagrams were obtained for the three configurations, the envelopes of which provide the limiting tool widths for stable machining without chatter (Figure 4.22). Figure 4.22

shows the eroded texture to provide a significant increase in the limiting width of cut relative to both the commercial (ground tool) and control (extruded aluminum) configurations. Indeed, the enhancement is more than a 100% relative to the commercial tool.

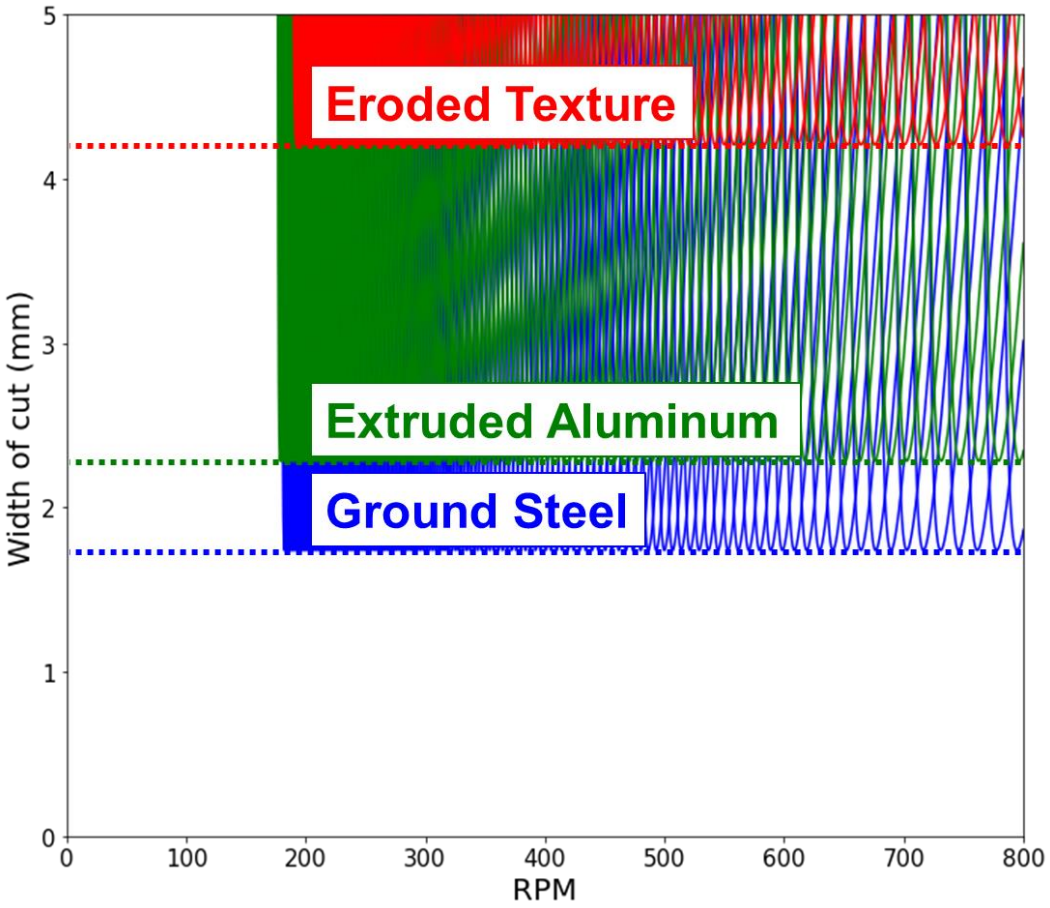

Figure 4.22 Stability limit plot for all three situations.

Grooving experiments were conducted to verify the stability plots for the control configuration (extruded aluminum) and the EDM textured setup, and to demonstrate the application potential of the technology developed in this thesis research. For these

experiments a blade holder with a 0.75-inch shank was mounted in a 1-inch tool holder, to allow for the placement of the insert below the blade holder and still maintain the correct center height. Given that the predicted stability limit was 4.1 mm for the eroded configuration and 2.3 mm for the control (extruded aluminum) configuration, a cutting insert with a cut width of 4 mm was chosen for the grooving experiments. The cutting experiments were conducted dry and involved an AISI 1020 workpiece of 63.5 mm diameter. The cutting speed was maintained constant at 165 m/min (to be above the range where process damping dominates) by making use of the constant surface speed capability of the CNC. The infeed was kept constant at 0.2 mm/rev. A comparison of the resulting surface finish in the machined grooves is shown in Figure 4.23 as an indication of the occurrence of chatter or the lack thereof.

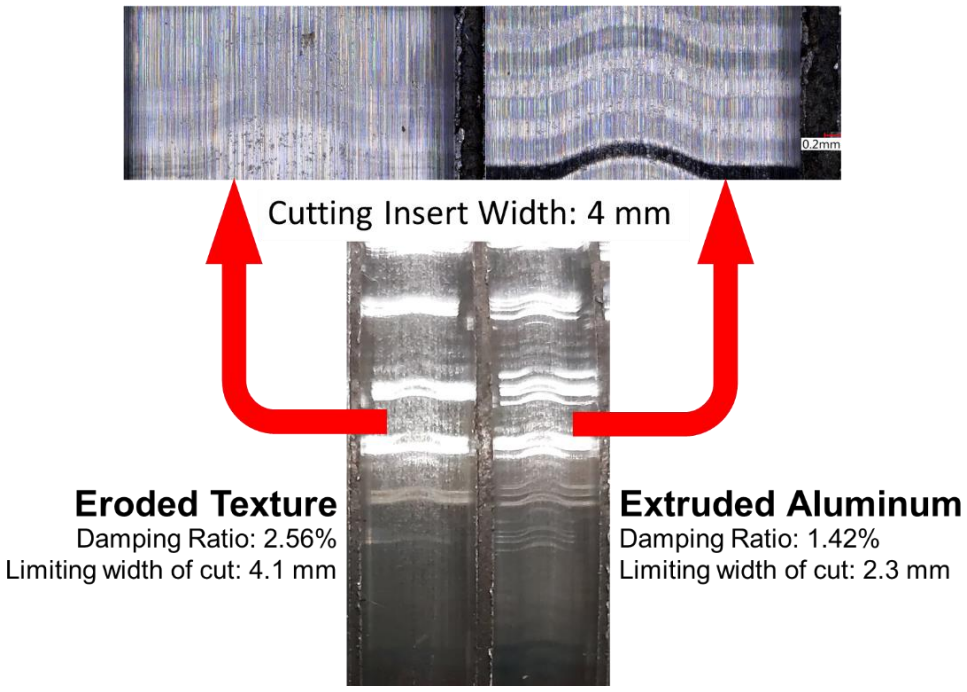

Figure 4.23 Comparison of surface finish of machined grooves.

Figure 4.23 shows severe chatter marks for the control configuration, exactly as predicted by the stability limit diagram. Chatter was but significantly alleviated by the configuration with the eroded textures; the presence of some feeble chatter in this case can be attributed to the insert width (4 mm) being close to the predicted theoretical stability limit (4.1 mm). It may be noted that for the chosen tool width of 4 mm, the commercial tool would be inherently unstable as indicated by the stability limit diagram. This set of experiments clearly demonstrates the efficacy of the technology developed in this thesis research to significantly enhance tool performance, without any required alterations to the tool as is the case of parting tools with a tuned mass damper.

Chapter 5

5 Conclusions and Future Work

5.1 Conclusions

This work was motivated by challenges in dynamic stability of grooving operations due to chatter. Various studies seeking to solve this problem by enhancing the damping of the tool system were investigated and their drawbacks explained. Enhancing damping by means of a passive frictional technique was proposed as an elegant and effective alternative. Several studies investigating the parameters that affect the performance of this technology were realized. The results obtained from these studies are listed below:

1. The effect of insert positioning was investigated using an experimental setup. It was shown that by placing an extruded aluminum insert on the top position of the setup a damping ratio of 0.51% was obtained and when placing the same insert on the bottom position, a damping ratio of 0.95% was obtained, showing the bottom position to be clearly favorable for this technique. An FEA model of the experimental setup was developed in order to investigate this difference in performance. Using the FEA model the reason

behind the performance difference was explained and proven to be the existence of a larger relative displacement leading to microslip between the insert and the steel beam, when the insert is place in the bottom position.

2. When conducting tap test in the direct FRF orientation, it was shown that a damping ratio of 1.12% can be obtained when having two cold rolled steel surfaces undergoing microslip. It was also shown that this will decrease to 0.95% if an extruded aluminum insert is placed between these two steel surfaces; even if using an optimum position shown to favor energy dissipation through microslip. Finally, it was shown that the damping ratio can be increased to 1.48% if the inserted aluminum piece is eroded using a discharge current of 39 A and a discharge duration of 365 μs. The eroded insert was able to enhance damping on the structure by 32 % when compared with no inserts being used and by 56% when extruded aluminum inserts were used. When conducting tap tests in the cross FRF orientation, it was shown that the 72 A and 65 μs texture is also able to enhance damping when compared with cold rolled steel surfaces and extruded aluminum surfaces, although by a different amount and with smaller damping ratios. It was concluded that the smaller damping values were caused by a smaller relative displacement between the insert and the steel beam. This smaller displacement comes from the steel beam having a higher bending stiffness along the cross FRF direction. With the cross FRF tap tests, the cold rolled surface corresponded to a damping ratio of 0.45% while the extruded aluminum obtained 0.51% and surface eroded with 72 A and 65 μs obtained 0.78%. This meant that in the cross FRF orientation, the eroded texture was able to enhance the structure damping by 73% when compared with the cold rolled steel surfaces and by 47% when compared with the extruded aluminum surface.

3. A surface texture eroded with a discharge current of 72 A and a discharge duration of 65 μs proved to achieve repeatable damping ratios when undergoing subsequent cycles of assembly and disassembly. Damping enhancements obtained by that surface texture were not affected after the texture was subjected to contact pressure twice as high. After 2 subsequent cycles of assembling with 11 Nm of tightening torque the surface texture still showed an average damping value of 2.5%. When assembled with a tightening torque of 21 Nm the surface showed an average damping value of 2% and when subsequently reassembled twice more using a tightening torque of 11 Nm, the surface showed and average damping ratio of 3% and then 2.5%.

4. Surfaces were machined with different values of discharge duration varying from 12 μs to 250 μs and with three different values of discharge current: 21 A, 39 A and 72 A. A balance between the two eroding parameters was found to be required in order to achieve the optimum damping value. This optimum value was found to shift following a pattern, where smaller values of current required larger values of discharge duration to achieve an optimum value of damping. From analyzing surface topographic characteristics as well as from data gathered in the literature, it was found that to achieve the optimum surface damping, a surface needed to have a large value of kurtosis as well as a large positive value of skewness. It was concluded that this combination of surface characteristics was responsible for the required balance between discharge duration and discharge current.

5. When varying the textured area on different aluminum inserts it was observed that higher damping values could be achieved with larger textured areas. Keeping the width on all inserts the same at 25 mm and eroding them all with 72A and 65 μs of discharge

duration. The effect of textured area was observed by varying the length of each insert. Lengths of 65, 73, 85, and 100 mm were tested. The longest insert was able to achieve a damping ratio of 4.5% while the smallest one achieved a damping ratio of 1.2%, this meant a damping enhancement of 3.75 times between the two lengths. Further studies are required to determine if this enhancement is caused by the difference in textured area, or by the difference in contact pressure.

6. It was proven that influencing pressure distribution in the contact area between two surfaces can increase damping originated from microslip. Holes of 5 difference sizes were drilled in identical inserts eroded with the same texture. The texture was machined with a discharge current of 72 A and a discharge duration of 65 µs. The number of drilled holes per insert varied in function of the hole size as to guarantee that the area reduction between every insert was always 25%. The best situation was composed of 32 holes, that were 4 mm in diameter. This combination achieved a damping enhancement of more than 4 times when compared with contacting cold rolled steel surfaces. With this experiment it was concluded that smaller holes can significantly increase damping ratio originated from microslip between textured interfaces. It was concluded that this phenomenon happens because at the edge of the drilled hole a stress applied tangentially to the contact area can surpass the frictional force present in that contact, causing microslip to happen at the area around the edge of the drilled hole. It was also concluded that smaller holes have better performance as more holes will fit in the same area, increasing the region where microslip can happen.

7. Stability limit diagrams were calculated for a grooving experimental setup in three situations. The first one where only ground surfaces were in contact. The second one

where only extruded aluminum inserts were contacting and a third one, where the same extruded aluminum inserts were eroded using a discharge current of 72A and discharge duration of 65 μs, with one of the inserts being drilled with 32 four mm holes. From this experiment it was concluded that using drilled and eroded inserts can increase the limiting width of cut by 127% when comparing with a situation where no inserts are used, as currently done in industry.

8.Grooving operations were conducted using a situation with only extruded aluminum inserts and a using a situation with eroded and drilled inserts. The eroded inserts had a texture made with 7 2A of discharge current and 65 μs of discharge duration. The drilled insert had 32 four mm holes. During this experiment the first situation chattered during grooving, this could be seen from the severe chatter marks left behind in the surface finish. The second situation was able to significantly alleviate chatter faced during the same grooving experiment, leaving only feeble chatter marks on the surface finish. It was concluded with this experiment that the eroded/drilled inserts can significantly alleviate chatter during grooving operations and thus enhance process stability without the need of significant alterations to the parting blade, nor any kind of prior tuning.

This work demonstrated the use of a novel approach for frictional damping of cutting tools using EDM surface texture and drilled holes. Eroded surfaces were tested in grooving operations and compared against surfaces with different textures, outperforming them all and showing to be capable of improving the dynamic stability of the system.

5.2 Future Work

In this section, future work that could advance the current understanding of microslip induced damping for EDM textures is suggested.

1. Section 4.1.5 presented an investigation regarding the effect of textured area on damping ratio. The results presented there show an increase in damping as the textured area increases. Because the tightening torque used in this experiment was constant for all different textured areas, larger areas were under smaller contact pressure. Other works [3][15][16][26] have shown that decreasing contact pressure can lead to increasing damping rations, thus the results presented in that section could also be attributed to the decrease in contact pressure as the textured area increased. An experiment where contact pressure is kept the same for all eroded areas would have to be realized in order to further investigate this effect.

2. During this research only Aluminum 6061 alloy inserts were studied. Other types of materials as different steel alloys could be tested as well, as to investigate if higher damping ratios could be achieved.

3. Surface textures exhibiting values of kurtosis and positive values of skewness higher than the ones achievable through EDM could be engineered and fabricated by other means as 3D printing or micro milling, in order to achieve higher damping ratios.

4. Eroding directly the parting blade or the blade holder, as well as other parts of the tool assembly could be investigated in order to determine if the process would be as

effective without the use of eroded aluminum inserts. This would streamline the technology making it simpler to implement in industry.

Chapter 6

6 References

[1] Sansmachining (2020). *How To Reduce Chatter & Vibration In CNC Machining*. [online] SANS. Available at: https://www.sansmachining.com/how-to-reduce-chatter-vibration-in-cnc-machining/ [Accessed 7 Sep. 2021].

[2] Panossian, H.V. (1992). Structural Damping Enhancement Via Non-Obstructive Particle Damping Technique.*Journal of Vibration and Acoustics*, 114(1), pp.101–105.

[3] Marui, E., Ema, S., Hashimoto, M. and Wakasawa, Y., 1998. Plate insertion as a means to improve the damping capacity of a cutting tool system. *International Journal of Machine Tools and Manufacture*,*38*(10-11), pp.1209-1220.

[4] Saffury, J. (2017). Chatter Suppression of External Grooving Tools.*Procedia CIRP*, 58, pp.216–221.

[5] Groper, M. (1985). Microslip and macroslip in bolted joints.*Experimental Mechanics*, 25(2), pp.171–174.

[6] Goyder, H.G.D. (2017). Damping Due to Joints in Built-Up Structures. *The Mechanics of Jointed Structures*, pp.135–147.

[7] Schmitz, T.L. and Smith, K.S. (2019). *Machining Dynamics*. Cham: Springer International Publishing.

[8] www.youtube.com. (n.d.). *Introduction to Iwan Models and Modal Testing for Structures with Bolted Joints*. [online] Available at: https://www.youtube.com/watch?v=hB0JOAdiBz8 [Accessed 7 Sep. 2021].

[9] Munoa, J., Beudaert, X., Dombovari, Z., Altintas, Y., Budak, E., Brecher, C. and Stepan, G. (2016). Chatter suppression techniques in metal cutting. *CIRP Annals*, *65*(2), pp.785-808.

[10] Lu, X., Chen, F. and Altintas, Y., (2014.) Magnetic actuator for active damping of boring bars. *CIRP Annals*, *63*(1), pp.369-372.

[11] Saleh, M.K., Nejatpour, M., Acar, H.Y. and Lazoglu, I., (2021). A new magnetorheological damper for chatter stability of boring tools. *Journal of Materials Processing Technology*,*289*, p.116-931.

[12] Iscar.com. (2017). *New Product Announcement*. [online] Available at: https://www.iscar.com/newarticles.aspx/countryid/1/newarticleid/2335 [Accessed 7 Sep. 2021].

[13] Biju, C.V. and Shunmugam, M.S. (2014) Investigation into effect of particle impact damping (PID) on surface topography in boring operation. *The International Journal of Advanced Manufacturing Technology*, *75*(5-8), pp.1219-1231.

[14] Ziegert, J.C., Stanislaus, C., Schmitz, T.L. and Sterling, R. (2006). Enhanced Damping in Long Slender End Mills. *Journal of Manufacturing Processes*, 8(1), pp.39–46.

[15] Hayati, S., Shahrokhi, M. and Hedayati, A. (2021). Development of a frictionally damped boring bar for chatter suppression in boring process. *The International Journal of Advanced Manufacturing Technology*, *113*(9), pp.2761-2778.

[16] Rogers, P.F. and Boothroyd, G. (1975). Damping at Metallic Interfaces Subjected to Oscillating Tangential Loads. *Journal of Engineering for Industry*, 97(3), pp.1087–1093.

[17] Marui, E., Ema, S. and Miyachi, R., (1994). An experimental investigation of circular saw vibration via a thin plate model. *International Journal of Machine Tools and Manufacture*, *34*(7), pp.893-905.

[18] Wentzel, H., Olsson, M. and Oberg, M. (2008). Metallic inserts as a tool to alter the structural damping of joined structures. *International Journal of Surface Science and Engineering*, *2*(1-2), pp.152-167.

[19] Medina, S., Olver, A.V. and Dini, D. (2012). The influence of surface topography on energy dissipation and compliance in tangentially loaded elastic contacts. *Journal of tribology*, *134*(1).

[20] Whitehouse, D.J. (2002). *Handbook of Surface and Nanometrology*. Taylor & Francis.

[21] Beards, C.F. and Neroutsopoulos, A.A. (1980). The Control of Structural Vibration by Frictional Damping in Electro-Discharge Machined Joints. *Journal of Mechanical Design*, 102(1), pp.54–57.

[22] Tlusty, J. (2000). *Manufacturing processes and equipment*. Upper Saddle River, NJ, Prentice-Hall.

[23] Tomlinson, G.A., (1929). CVI. A molecular theory of friction. *The London, Edinburgh, and Dublin philosophical magazine and journal of science*, *7*(46), pp.905-939.

[24] Budynas (2010). *Shigleys mechanical engineering design, 9th ed.* Mc Graw Hill.

[25] Stachowiak, G, Batchelor, AW, Stachowiak, G & Dowson, D (ed.) (2004), *Experimental Methods in Tribology*. vol. 44, 1st ed, Elsevier, Amsterdam, Netherlands.

[26] Ito, Y. and Masuko, M. (1975). Study on the Damping Capacity of Bolted Joints Effects of the Joint Surfaces Condition. Bulletin of JSME, 18(117), pp.319–326.